Department of Civil and Environmental Engineering

Assessment of air void content of asphalt using dielectric constant measurements by GPR and with VNA

Terhi Pellinen, Pekka Eskelinen
Eeva Huuskonen-Snicker, Ari Hartikainen

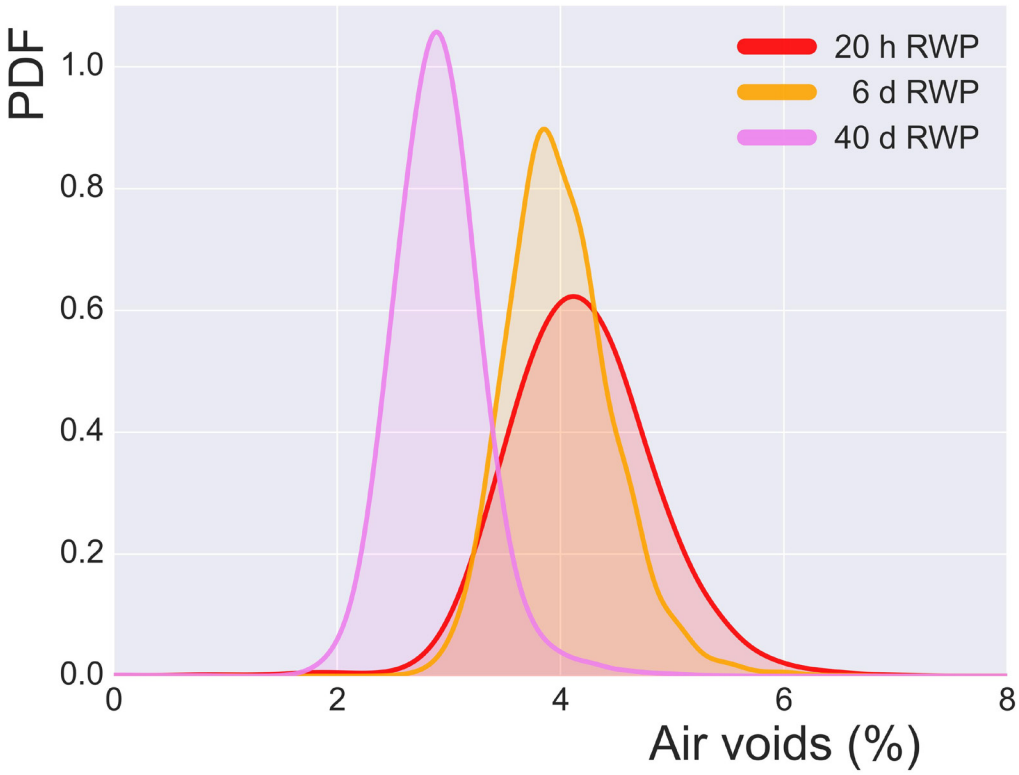

Aalto University
SCIENCE + TECHNOLOGY
RESEARCH REPORT

Aalto University publication series
SCIENCE + **TECHNOLOGY** 9/2015

Assessment of air void content of asphalt using dielectric constant measurements by GPR and with VNA

Terhi Pellinen
Pekka Eskelinen
Eeva Huuskonen-Snicker
Ari Hartikainen

Aalto University
School of Engineering
Department of Civil and Environmental Engineering
Highway Engineering

Aalto University publication series
SCIENCE + **TECHNOLOGY** 9/2015

ISBN 978-952-60-6288-4 (pdf)
ISSN-L 1799-4896
ISSN 1799-4896 (printed)
ISSN 1799-490X (pdf)
http://urn.fi/URN:ISBN:978-952-60-6288-4

Unigrafia Oy
Helsinki 2015

Finland

Author

Autor(s): Terhi Pellinen, Pekka Eskelinen, Eeva Huuskonen-Snicker, Ari Hartikainen

Name of the publication

Assessment of air void content of asphalt using dielectric constant measurements by GPR and with VNA

Publisher School of Engineering

Unit Department of Civil and Environmental Engineering

Series Aalto University publication series SCIENCE + TECHNOLOGY 9/2015

Field of research Highway Engineering

Abstract

For several years, Ground Penetrating Radar (GPR) has been used in Finland to evaluate the air void content of asphalt pavements. Air void content is an important quality measure of pavement condition for both old and new asphalt pavements. The objective is to investigate if the existing GPR technique and application employed in Finland is sufficiently accurate to be used as a quality control tool in assessing the compaction of newly laid asphalt pavements. The work comprised field and laboratory experiments and a review of the existing PANK calibration method for the GPR measurements. Field experiments were conducted in the summer of 2013 on highways Vt3 and Vt12, near the City of Tampere. The test roads were paved with SMA16 using an approx. 40 mm thick layer of new asphalt. Roads were measured with GPR several times during the fall of 2013. A total of 36 cores and 2 slabs were obtained from the roads and tested in the laboratory with a Vector Network Analyzer. Measurements were done with a 7 to 17 GHz transmission configuration to measure the reference dielectric constant of the asphalt mixture. A major finding is that the PANK calibration method for the GPR inadvertently reduces observed density variations and may introduce a systematic bias. This makes pavements appear to be more homogenous and dense than they actually are according to conventional measurements.

Keywords asphalt, air voids, GPR, permittivity, calibration, dielectric constant

ISBN (printed)	**ISBN (pdf)** 978-952-60-6288-4	
ISSN-L 1799-4896	**ISSN (printed)** 1799-4896	**ISSN (pdf)** 1799-490X
Location of publisher Helsinki	**Location of printing** Helsinki	**Year** 2015
Pages 75+2	**urn** http://urn.fi/URN:ISBN:978-952-60-6288-4	

TABLE OF CONTENTS

GLOSSARY OF ACRONYMS

AC	Dense graded mixtures
ALL	Modified Böttcher model, a model proposed by Al Qadi et al.
CRIM	Complex Refractive Index model
FAS	Finnish Asphalt Specifications
FTA	Finnish Transport Agency
GPR	Ground Penetrating Radar
LLL	Landau-Lifshitz-Looyenga mixing model
MA	Mastic asphalt
MVE	Measured volume element
NDT	Non-Destructive Testing
PA	Porous asphalt
QC/QA	Quality Control / Quality Assurance
REM	Hot in-place remix paving method
RVE	Representative volume element
SMA	Stone Mastic Asphalt
SSD	Saturated surface dry method
VFA/ VFB	Voids Filled with Bitumen
VMA	Voids in Mineral Aggregate
VNA	Vector Network Analyzer

GLOSSARY OF SYMBOLS

f	Frequency
A	Amplitude
φ	Phase
τ	Pulse duration
ρ	Density
ρ_p	Bulk density
ρ_m	Maximum density of loose mixture
V_a	Air void content, (%)
σ	Electrical conductivity
ε_r^*	Complex dielectric constant (also relative permittivity)
ε_r'	Dielectric constant, real part
ε_r''	Dielectric constant, imaginary part
ε_0	Dielectric constant of free space, $8{,}8541878 \ldots \cdot 10^{-12}\ \mathrm{F/m}$
μ^*	Complex permeability
μ_0	Magnetic permeability of free space, $4\pi \cdot 10^{-7}\mathrm{N/A^2}$
c_0	The speed of light in vacuum, $299\ 792\ 458\ \mathrm{m/s}$
c	The speed of light in material
v	Wave velocity in material
λ	Wavelength of electromagnetic wave
Γ	Reflection coefficient
$\mathrm{A_r}$	Reflected amplitude
$\mathrm{A_0}$	Incident amplitude
θ_t	Angle of transmission
θ_i	Angle of incidence
η	Impedance
V_s	Volume of rock aggregate
V_b	Volume of bitumen in the pavement
ε_a^*	The complex permittivity of air-particle mixture
G_{mb}	Bulk specific gravity, see ρ_p
G_{mm}	Maximum specific gravity, see ρ_m
G_{se}	Effective specific gravity aggregates
P_b	Asphalt binder content, (%)
$\mathrm{P_s}$	The percentage of aggregate in the mixture
σ_{GPR}	Standard deviation of permittivity obtained by GPR
R^2	Coefficient of determination
k	Calibration factor
Ø	Diameter of the core

FOREWORD

This report presents findings from Phase I of the study on *Assessment of Asphalt Pavement Density* (Tiiveyden mittauksen ja arvioinnin kehittäminen) included in the *Pavement Life Cycle Research Program, 2013-2017* (Elinkaaritehokas tiepäällyste, 2013-2017) commissioned by the Finnish Transport Agency (FTA). The FTA program officer is Pavement Engineer, Katri Eskola, and from Aalto University, the PI of the project is Prof. Terhi Pellinen. The research is a collaboration between the Civil Engineering Department and the Department of Electrical Engineering and Automation, where Prof. Pekka Eskelinen is in charge of electromagnetic measurements and research. Doctoral students, Eeva Huuskonen-Snicker, M.Sc (Tech.) and Ari Hartikainen, M.Sc (Tech.), have contributed to the analysis of the VNA and GPR data as well as to the preparation of this report.

The authors wish to thank Pablo Olmos Martinez, M.Sc. (Tech.) and Antti Kuosmanen, M.Sc. (Tech.) for the collection of field samples and the analysis of REM contracts and GPR data; Kalle Kanervo, M.Sc. (Tech.) and doctoral student Martta-Kaisa Olkkonen, M.Sc. (Tech.) for the help they have provided in the data analysis; as well as undergraduate student, Jussi Eskelinen, for his help in finalizing the report.

TIIVISTELMÄ

Maatutkaa (Ground Penetrating Radar, GPR) on käytetty Suomessa pitkään asfalttipäällysteiden tyhjätilan määrittämiseen. Tyhjätila on tärkeä kriteeri sekä uusien että vanhojen asfalttipäällysteiden laadun selvittämisessä. Tavoitteena on tutkia, onko Suomessa tällä hetkellä käytössä oleva GPR-tekniikka ja sen soveltaminen tarpeeksi tarkkaa uusien asfalttipäällysteiden tiiveyden mittaamiseen. Työ koostui kenttä- ja laboratoriotutkimuksista sekä GPR-mittausten kalibrointiin käytetyn PANK-kalibraatiomallin arvioinnista. Kenttäkokeet suoritettiin kesällä 2013 Tampereen lähellä valtateillä 3 ja 12. Teiden päällyste oli tyypiä SMA16, ja uuden asfalttikerroksen paksuus oli 40 mm. Tiet mitattiin 1 GHz maatutkalla useita kertoja syksyn 2013 aikana. Teiltä otettiin 36 poranäytettä ja 2 laattanäytettä jotka testattiin laboratoriossa vektoripiirianalysaattorilla. Asfalttiseoksen dielektrisyysvakio mitattiin 7-17 GHz läpimittauskonfiguraatiolla vertailuarvojen saamiseksi. Tärkein havainto oli se, että PANK-kalibraatiomallin käyttö maatutkamittauksissa vähentää havaittuja tiheyden vaihteluita ja saattaa lisätä systemaattisen virheen mittauksiin. Tämä saa päällysteet näyttämään tasalaatuisemmilta ja tiiviimmiltä kuin mitä ne oikeasti ovat.

1 INTRODUCTION

1.1 Scope and objectives

Since the 1980s, ground-penetrating radar (GPR) has been used in Finland for civil engineering applications. Common GPR applications in road surveys, include thickness evaluation of the pavement, subgrade soil evaluation, and evaluation of soil moisture and frost susceptibility. GPR has also been used to evaluate the air void content of asphalt pavements for several years. Air void content is an important quality measure of pavement condition for both old and new asphalt pavements. The Finnish guidelines and PANK specifications for the method were released in 1999. The GPR measures the dielectric constant ε_r' of the asphalt, which is then correlated to the air void content. To obtain the air void content, a few pavement cores must be drilled for calibration.

However, the accuracy of the method has recently been called into question for two reasons: first, this method of calibration may inadvertently reduce density variations and cause systematic bias, which makes pavements appear to be more homogenous and dense than they actually are; secondly, the frequency range used may not have adequate depth resolution for separating the thin asphalt surface layer from the rest of the pavement structure.

The objective of the *Assessment of Asphalt Pavement Density* study is to investigate if the existing GPR technique employed in Finland is accurate enough to be used as a Quality Control/Quality Assurance (QC/QA) tool in assessing the compaction of newly laid asphalt pavements. The work consisted of field and laboratory experiments and a review of the existing PANK calibration method for the GPR measurements.

Field experiments were conducted in the summer of 2013 on highways Vt3 and Vt12, near the City of Tampere. The test roads had two lanes for one direction and roads were paved with the Stone Mastic Asphalt mixture SMA16 with a 40 mm thick new pavement layer. A total of 36 cores and 2 slabs were obtained from the roads and tested in the laboratory for their air void contents. In addition, raw materials were collected from the quarry and the asphalt plant for further permittivity studies.

As a reference independent of the GPR, the field GPR measurements were compared with the Vector Network Analyzer (VNA) measurements conducted in the laboratory of Electrical Engineering at Aalto University. Vector network analysis is a method of accurately characterizing signal deformations by measuring their effect on the amplitude and phase of swept-frequency test signals. The VNA measurements can then be considered to give the actual permittivity values; therefore, they should set the baseline for evaluating the GPR measuring technique. The VNA used in this research was the Wiltron 360 Network Analyzer model.

There are two basic principles of measuring material permittivity with an electromagnetic wave, transmission and reflection configuration. In this work, two waveguide antennas that operate in the frequency band of 7-17 GHz will be used in both the transmission and reflection configuration. The beam width (footprint) of the antennas is approximately a circle with a 20 mm diameter on the sample surface. In the transmission configuration, the antennas are on both sides of the sample. This is only suitable for laboratory testing. For field pavement applications, the radar scanning must be conducted using reflection measurements.

The reasons for using the microwave frequencies of 7 to 17 GHz in laboratory studies is the need for a better depth or “thickness” resolution in the permittivity measurements. The

additional advantage this provides is that the antenna size is smaller, which enables the measurement of pavement cores.

1.2 Volume bulk property

The GPR transmits electromagnetic waves into the ground and records the echo characteristics, such as amplitude and time delay. To obtain the dielectric material property in this case, the real part of relative permittivity ε_r', the measured electromagnetic quantities, amplitude (A) and phase (φ) must be converted to ε_r' via radar electronics calibration. This is usually done with a metal plate. The principles of reflectivity calibration are explained in detail, for example, in Scheer (1983). Then, to obtain a conventional material property, such as density (ρ), another calibration is needed to correlate the physical measurements and the radar measurements.

The total thickness of bound asphalt concrete layers can range from 40 to more than 200 millimeters depending on road classification and traffic volumes. At low traffic volumes, for roads where the asphalt concrete thickness is less than 130 mm, the depth resolution of the GPR may reach down to unbound aggregate base layers. The dielectric constant of asphalt is obtained from the signal reflecting from the surface as is schematically shown in Figure 1 below. For 2.2 GHz antennas, the scanned footprint area is 300 x 300 mm. In the continuous measuring mode, the GPR used in the experiment took ten scans per meter to produce one data record per meter, which covers 0.3 m x 1 m area. Depending on the attenuation of the signal, it is possible that multiple reflections are recorded which then interfere with the surface reflection. Therefore, in addition to averaging air voids over spatial area, the measured ε_r' covers a "volume bulk property" for the asphalt surface layer and different layers below it, as Figure 1 below illustrates.

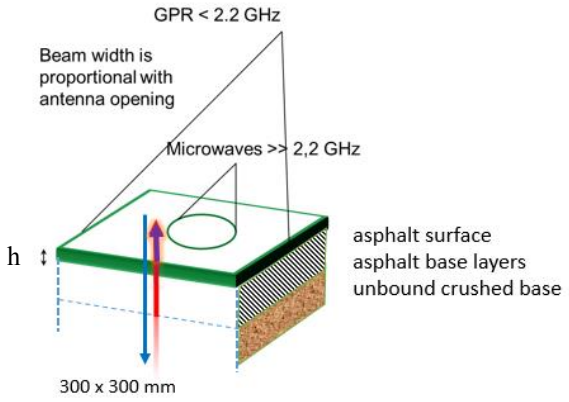

Figure 1. *The radar wavelength should be shorter than the thickness of the surface layer to prevent multiple reflections.*

A core, drilled from the asphalt pavement, represents a discrete point measurement. Depending on the homogeneity of the pavement, the antenna footprint of 300 x 300 mm may cover variable material properties. Therefore, a representative volume element (RVE) must be determined to quantify this variation for the assessment of paved road quality.

Thus, a coring plan was developed to study the spatial variation of the air voids of asphalt in the GPR measurement area. Although quality measurements are obtained from the right wheel path, it was decided to investigate both the wheel path and the center of the road. In this way, we would have a reference location which should not have densification due to traffic.

1.3 Asphalt pavement homogeneity

The magnitude of the pavement non-homogeneity depends on the level of physical segregation of the mixture. Studies show (Pellinen, 1985; Stroup-Gardiner and Brown, 2001; Nevalainen 2014) that asphalt pavement suffering from truck load-end segregation may have variation in the binder content up to ±1.5 % depending on the mixture type. The air voids variation may be confounded by the thermal segregation, but variation from zero to 5 - 6% within less than a 10 meter distance is quite typical. Figure 2 shows truck load-end segregation of SMA16 mixture detected by the thermal camera from a recent study by Nevalainen (2014). Cores taken from the coarse portions (21 to 24 and 29 to 32) and from the fine portion (25 to 28) of the segregated truck loads reveal the variation of binder content and air voids with the subsequent calculated volumetric quantities of Voids in Mineral Aggregate (VMA) and Voids Filled with bitumen (VFA).

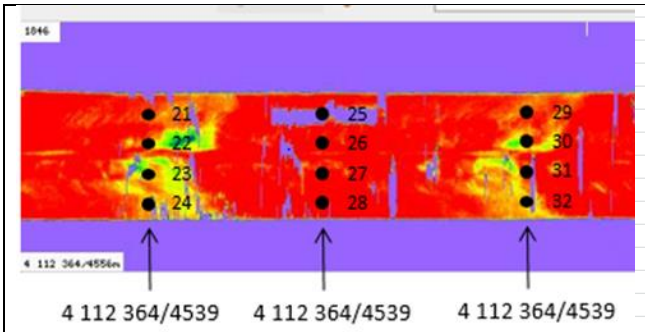

Core No	Pb%	Va%	VMA%	VFA%
21	5,5	3,3	15,15	78,46
22	5,4	3,6	15,03	76,13
23	5,5	0,6	12,87	95,48
24	4,7	2,7	13,65	80,04
25	5,5	1,0	13,47	92,74
26	5,3	0,0	12,44	100,00
27	6,4	2,7	14,61	81,36
28	5,2	2,0	13,30	85,21
29	6,0	5,7	15,60	63,23
30	5,1	6,8	14,78	53,83
31	5,4	3,1	14,34	78,28
32	5,1	2,4	12,87	81,54
Max	*6,4*	*6,8*	*15,60*	*100,00*
Min	*4,7*	*0,0*	*12,44*	*53,83*
Range	*1,7*	*6,8*	*3,16*	*46,17*

Figure 2. *Truck load-end segregation of SMA 16 mixture detected by thermal camera (replicated from Nevalainen, 2014).*

2 GPR FOR PAVEMENT INVESTIGATIONS – GENERAL BACKGROUND

2.1 Theory

The propagation and attenuation of the electromagnetic field depend on the electrical and magnetic properties of the medium, which are electrical conductivity σ, dielectric permittivity $\varepsilon^*$and magnetic permeability μ^* (Annan, 2003). In this study, we focus only on dielectric permittivity as magnetic properties (i.e., permeability) can be neglected for aggregates of this type (Huuskonen-Snicker et al. 2015). Permittivity ε^* is a complex variable

$$\varepsilon^* = \varepsilon_0 \varepsilon_r = \varepsilon_0(\varepsilon_r' + j\varepsilon_r''), \quad (1)$$

where ε_0 is the permittivity of free space, ε_r relative permittivity of material, ε_r' is real part of relative permittivity and ε_r'' is imaginary part of relative permittivity. The real part of frequency dependent relative permittivity describes the stored energy and the imaginary part accounts for energy losses in the medium.

The speed of electromagnetic radiation depends on the electric and magnetic properties of the medium traversed. The velocity in vacuum c_0 is given by vacuum permittivity ε_0 and permeability μ_0.

$$c_0 = \sqrt{1/(\varepsilon_0 \mu_0)} \approx 3 \times 10^8 \, m/s \quad (2)$$

For light or radio waves in a medium, permeability is normally 1 in practically all materials of interest. Different optical (or wave propagation) properties of materials arise from differences in permittivity. The permittivity of material is denoted in Eq. (3), where the dielectric constant or relative permittivity ε_r is a material property. Thus velocity *v* in a medium is

$$v = c_0/\sqrt{\varepsilon_r} \quad (3)$$

The value of the dielectric constant is related to the tendency of the electric field (voltage) to cause significant polarization or charge redistribution in a material. As ε_r thus involves various phenomena, such as rearrangement of dipoles or movement of electrons, it is understandable that dielectric charge redistribution does not necessarily follow changes in the driving electric field instantaneously. It follows that for an oscillating electric field, the value of the dielectric constant depends on the frequency *f* of the oscillations; generally a higher frequency leads to a lower $\varepsilon_r(f)$.

When any wave motion crosses a threshold where the dielectric constant changes, one part of the wave is reflected and another part is refracted. The intensities of the reflected and refracted waves depend on changes in ε_r' and on the angle of incident between the direction of propagation and the threshold. The study of reflected waves allows the detection of boundaries between material layers with different dielectric constants. Reflection intensities allow the estimation of dielectric constants and these combined with knowledge about time intervals between different reflections enable the estimation of layer thickness.

If the medium the wave propagates through is not homogenous, the medium contains – in principle – numerous reflecting/refracting boundaries. In practice, however, when the size scale of the variations in composition is smaller than the wavelength, wave interaction with individual "grains" is very limited and the wave propagation can be considered to be occurring in a medium with effective permittivity roughly corresponding to the volume averaged permittivity

of its component materials. This is discussed in more detail in Section 2.2. The wavelength for electromagnetic waves is:

$$\lambda = v/f = c_0/(f\sqrt{\varepsilon_r}) \quad (4)$$

2.2 Current GPR devices

The main technical parameters of a GPR system regarding road pavement measurements are:

- operating center frequency (e.g. 1 or 2,2 GHz)
- equivalent pulse width (e.g. 1 ns)
- dynamic range (e.g. 40 dB)
- setting an attenuation limit z
- illumination area on asphalt surface (e.g. 0,3 m x 0,3 m)
- amplitude stability (e.g. 1 dB)

Lower frequency GPR sets are originally designed for the relatively deep probing of soil, down to 6 meters or more. In this case, attenuation in rock and clay, for example, calls for low carrier frequency, typically up to 2.2 GHz. However, a physical limitation is now met requiring obtainable depth resolution, because the spectrum created by pulsing the transmitter of radar can exceed considerably "above" the nominal carrier. From signal frequency theory (Barton, 2005), we ascertain that a pulse of duration τ requires, just for its first spectral component, a bandwidth of $2/\tau$. Thus, for a 2.2 GHz radar we are limited to about 1 ns, the obtainable depth resolution is thus close to 0.3 m in air, for example, and ca. 0.13 m in asphalt.

The commercial GPR devices measure the amplitude and the delay of the reflected waves. The dielectric value can be calculated by using the reflection coefficient. This coefficient can be calculated using the incident amplitude and the reflected amplitude, assuming just one boundary between two semi-infinite regions.

$$\Gamma = A_r/A_0 \quad (5)$$

where

Γ	reflection coefficient
A_r	reflected amplitude [V]
A_0	incident amplitude.

The coefficient of reflection can also be derived by applying basic electromagnetic theory and the boundary conditions at the surface. The reflection coefficient can then be calculated using Eq. (6) (Lahouar 2003).

$$\Gamma = \frac{-\eta_1 \cos\theta_t + \eta_2 \cos\theta_i}{\eta_1 \cos\theta_t + \eta_2 \cos\theta_i} \quad (6)$$

where

$\eta_{1,2}$	impedance of the material
θ_t	angle of transmission
θ_i	angle of incidence

Impedance is related to permeability and permittivity as

$$\eta = \sqrt{\mu^*/\varepsilon^*} \tag{7}$$

Because the radar antennas are perpendicular to the asphalt, the angle of transmission and incidence are equal to 90 degrees. The magnetic permeability is assumed equal to one. That means no significantly magnetic materials are present in the asphalt. If we combine (6) and (7), we get the reflection coefficient as

$$\Gamma = \frac{\sqrt{\varepsilon_1} - \sqrt{\varepsilon_2}}{\sqrt{\varepsilon_1} + \sqrt{\varepsilon_2}} \tag{8}$$

Let us now assume that the upper half-space is filled with material 1 and the lower with material 2. The two materials involved are air and asphalt. The relative permittivity of air is constant and equals to 1. Eq. (9) shows the final result.

$$\varepsilon_r = \left[\frac{1 + {}^{A_r}/_{A_0}}{1 - {}^{A_r}/_{A_0}}\right]^2 \tag{9}$$

where

A_0	incident amplitude
A_r	reflected amplitude
ε_r	permittivity of asphalt

The incident amplitude is obtained with a metal plate. The antennas are placed on top of the metal plate, which can be assumed to give a perfect reflection of 1 (Figure 3). The reflection is measured and used as the incident amplitude.

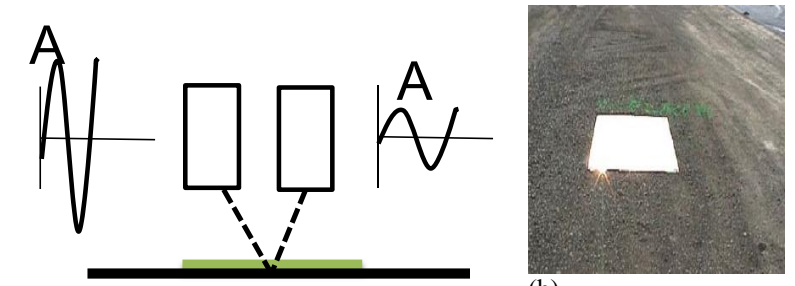

(a) (b)

Figure 3. a) *Schematic of GPR measurement; b) reflection (calibration) plate.*

2.3 Simulation of depth resolution

The depth resolution of a GPR system can be simulated with transmission line models. For the purpose of this study, we created the schematic of Figure 4. Here we assume that the GPR antennas are 300 mm above the asphalt surface and that the half power pulse width of the radar

is 1 ns. Different short pieces of transmission line can then be added one after the other to the model in order to mimic the actual road structure. For example, in Figure 4, we illustrate a general situation with two asphalt layers (4 cm with ε_r'=5 and 5 cm with ε_r'=6) above infinite supporting soil mass with ε_r'=7. For computing a reference value, we first remove the lower asphalt and the supporting layer and assume that the top asphalt, having a dielectric constant ε_r' of 5.0, fills the entire volume below the antennas down to infinity. This gives us the true reflection amplitude of 385 mV as indicated in Figure 5. Then we change the configuration creating two asphalt layers (but no supporting mass), the first 4 cm thick (ε_r'=5) and another below it down to infinity (ε_r'=4). If the pulse width is still 1 ns, the obtained first reflection amplitude is wrongly 368 mV as is shown in Figure 6. Finally, in Figure 7, we shorten the radar pulse to 100 ps (at half power bandwidth) and, with the same two asphalt layer configuration receive again the true reflection amplitude. If the wrong amplitude of 368 mV is used in further analysis, we receive instead of ε_r'=5 a falsified value of ε_r'=4.7. For the simulated pavement structure shown in Figure 4, the ε_r' values become 5.2.

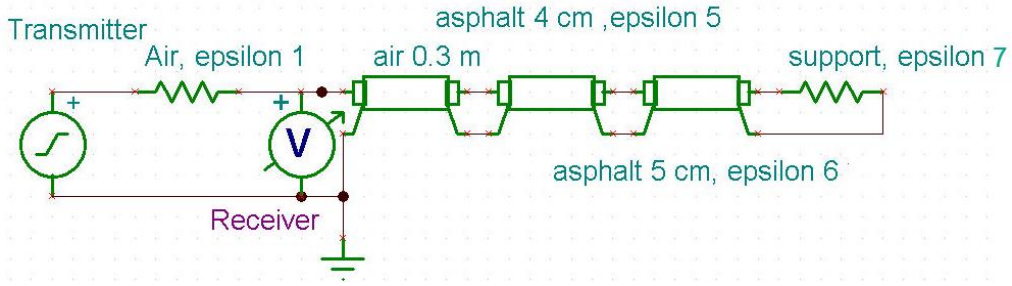

Figure 4. *Simulation model for GPR pulse width effects.*

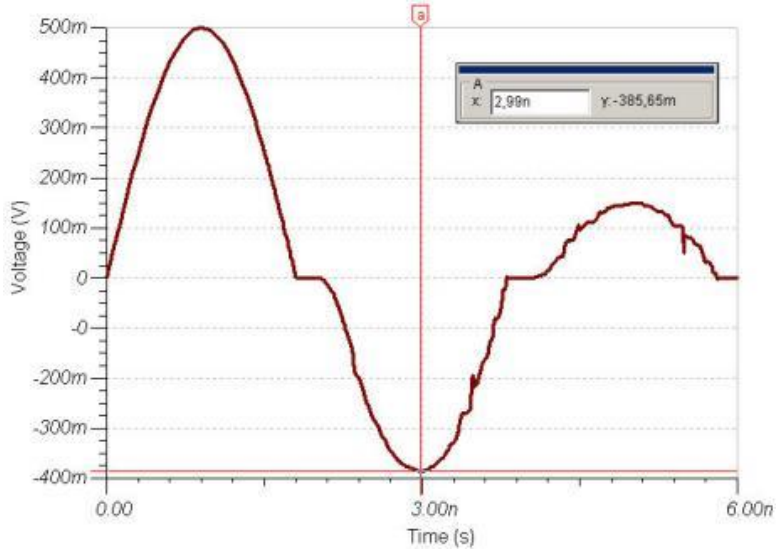

Figure 5. *Simulated response for infinitely thick asphalt with ε'=5 and 1 ns GPR pulse.*

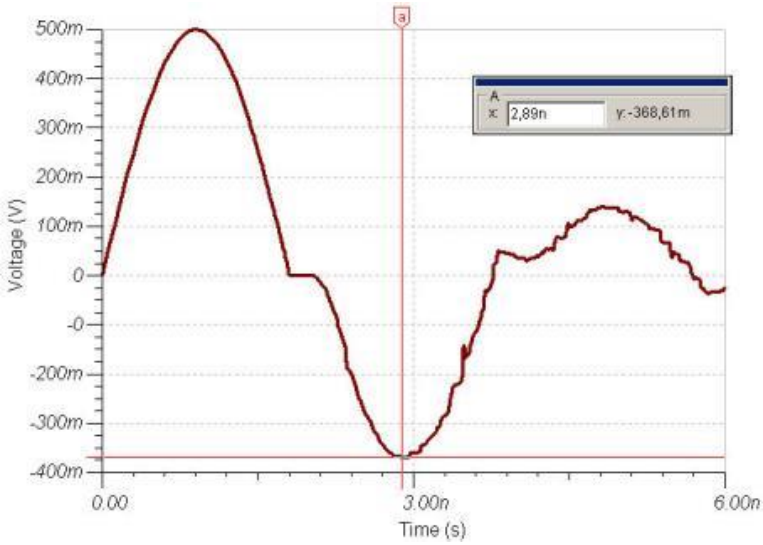

Figure 6. *Simulation result when 4 cm of asphalt (ε'=5) is above an infinite layer of ε'=4.*

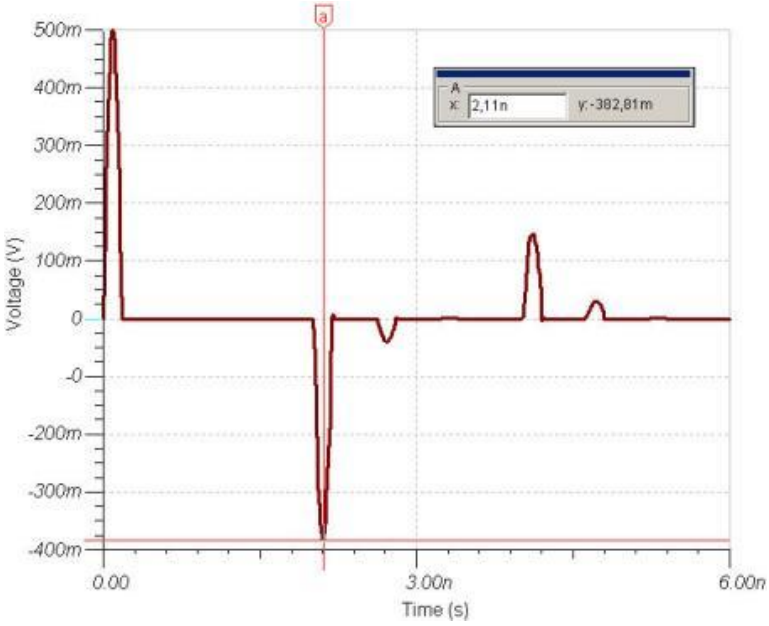

Figure 7. *Simulation result for the same configuration as in Figure 4 but now the GPR pulse is 100 ps.*

Typical GPR systems measure the magnitude of the reflected wave in order to get an estimate of the pavement permittivity. Figure 8 shows the dramatic effect of level measuring uncertainty ΔP in the observed dielectric constant for three nominal values (ε_r' = 3.1, 3.7 or 5.0). Interestingly, the relative error increases as the nominal permittivity grows. General microwave engineering technology is considered to be of good quality (at 1-2 GHz) when the level error stays within ±0.5 dB of the true value. The best commercial laboratory instruments seldom achieve this limit although they are operated in stable environmental conditions.

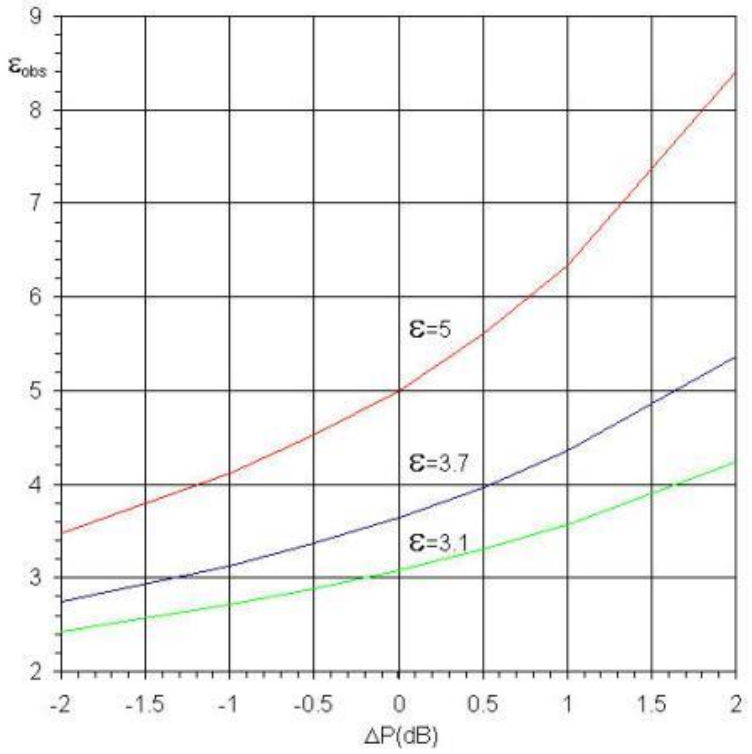

Figure 8. *Observed pavement permittivity as a function of GPR level measuring error for three different nominal values of the dielectric constant.*

3 EFFECTIVE PERMITTIVITY

3.1 Modeling of effective bulk properties

Asphalt is a composite material with aggregates, bitumen and air. The effective, bulk dielectric properties of composite materials are determined by the dielectric properties of its components. As studies show (Nelson, 2005), when pulverized granular materials are measured with RF or microwave frequencies the permittivity and density relationship can be expressed by mixing equations, such as Complex Refractive Index (CRIM) model or Landau & Lifshitz, Looyenga model (LLL). Different mixing formulas in respect to asphalt have been studied by (Leng, 2011; Leng et al. 2011; Al-Qadi et al. 2001). One of the simplest ones, Eq. (10) is the CRIM, where ε'_{reff} is the effective dielectric value obtained by combining material components with volume portions: V_a is volume of air, V_s is volume of rock aggregate and V_b is volume of bitumen in the pavement.

$$\sqrt{\varepsilon'_{reff}} = V_a\sqrt{\varepsilon'_{ra}} + V_s\sqrt{\varepsilon'_{rs}} + V_b\sqrt{\varepsilon'_{rb}} \tag{10}$$

Another simple model counting air-particle mixture density variations is given by Nelson (2005) based on the Landau & Lifshitz, Looyenga model where ε^*_a is the complex permittivity of air-particle mixture at given density ρ_a, and ε^*_b is the permittivity of the mixture at a different density ρ_b.

$$\varepsilon^*_b = \left[\left(\left(\varepsilon^{*\frac{1}{3}}_a - 1\right)\rho_b\right)/\rho_a + 1\right]^3 \tag{11}$$

A model proposed by Al Qadi et al. (Leng et al, 2011) is the ALL model, where bulk density of asphalt is calculated based on effective ε'_r of asphalt and its volumetric components, Eq. (12).

$$G_{mb} = \frac{\frac{\varepsilon_{AC} - \varepsilon_b}{3\varepsilon_{AC}} - \frac{1 - \varepsilon_b}{1 + 2\varepsilon_{AC}}}{\left(\frac{\varepsilon_s - \varepsilon_b}{\varepsilon_s - 2\varepsilon_{AC}}\right)\left(\frac{1 - P_b}{G_{se}}\right) - \left(\frac{1 - \varepsilon_b}{1_s + 2\varepsilon_{AC}}\right)\left(\frac{1}{G_{mm}}\right)} \tag{12}$$

where

G_{mb}	bulk specific gravity
G_{mm}	maximum specific gravity
G_{se}	effective specific gravity aggregates
P_b	asphalt binder content, %
ε_{AC}	asphalt concrete permittivity
ε_b	bitumen permittivity
ε_s	aggregate permittivity

Electromagnetic asphalt modeling is quite complicated and the influence of aggregates dominates the dielectric value of this composite. However, the dielectric properties of aggregates are not well reported and many researchers have only back-calculated the value from the asphalt dielectric bulk properties (Leng et al. 2011). This may lead to large errors in assessing pavement density. Thus, although dielectric constant is referred to, the properties for rock types are not constant as they vary depending on the mineralogy of the rock type. The ε'_r for typical aggregates is 4.5 to 6.5 (Saarenketo, 2006) with French researchers (Fauchard et al.

2013) reporting values ranging from 4.5 to 7.7. The bitumen ε_r' is reported to vary between 2.6 and 2.8 (Saarenketo, 2006).

3.2 Bulk volumetric proportions of asphalt

To obtain the air void content of asphalt, one has to first measure pavement density. There are several methods of obtaining pavement density for asphalt depending on the asphalt mixture type. Based on the gradation and packing of aggregates, asphalt mixtures can be categorized into four different types as seen in Figure 9 below.

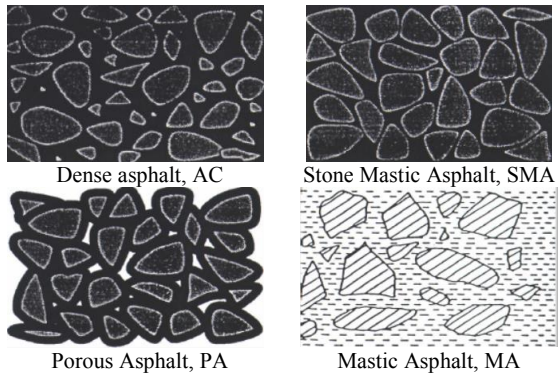

Figure 9. *Asphalt mixture types and their aggregate packing arrangements.*

The most used mixtures are the dense graded mixtures (AC), which are proportioned to have tight aggregate packing. The Stone Mastic Asphalt (SMA) is a heavy duty mixture with a strong aggregate skeleton filled with bitumen rich mastics. Porous asphalt (PA) has a similar aggregate skeleton, but without mastics, as this mixture is intended to be water permeable. Porous asphalt is a popular surface mixture in Europe for motorways as it drains itself and in this way prevents splash and spray as well as hydroplaning. In the mastic asphalt (MA), all the voids are filled with mastic and there are no air voids in the mixture. MA is self-leveling and roller compaction is not needed.

All these mixtures have different volumetric requirements. Figure 10 shows some typical values based on Finnish Asphalt Specifications (FAS, 2011). The weight-volume relationships and subsequent volume-related quantities in the asphalt mixture are the Voids in Mineral Aggregate (VMA), the Voids Filled with Bitumen (VFB) and the air void content (V_a). These quantities are calculated from the volume of bitumen and the volume of aggregate blend. The VMA varies between 15 to 30% and the volume of air may range from zero to 22 – 25% as is illustrated in Figure 10. The air void content, V_a in percent, is the ratio of the asphalt pavement density (ρ_p) and the maximum density (ρ_m), Eq. (13) and VMA is shown in Eq. (14) where (ρ_s) is the aggregate solid density and P_s is the percentage of aggregate in the mixture.

$$V_a = \left(1 - \rho_p/\rho_m\right) \cdot 100 \tag{13}$$

$$VMA = \left(1 - \frac{P_s \rho_p}{\rho_s}\right) \cdot 100 \quad (14)$$

A requirement for asphalt density is placed for the air void content. It has to be less than 5 to 6 % to have a durable impervious pavement, which can withstand freeze and thaw conditions. With the development of nondestructive testing (NDT) methods, there has been a gradual shift from the conventional destructive quality control/quality assurance (QC/QA) methods to these new techniques. Loizos and Plati (2011) have investigated the assessment of asphalt air voids and stiffness based on asphalt dielectric values. However, their models do not count for the rock aggregate type variation.

	MA (dry)	AC (dry)	SMA (SSD)	SMA(DIM)	PA (DIM)
V, bitumen	25	13	15	15	8
V, air	0	2	3	10	22
V, stone	75	85	82	75	70
VMA	25	15	18	25	30

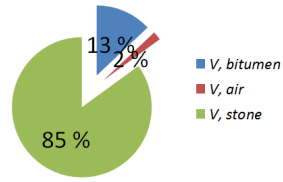

Figure 10. *Typical volumetric properties (percentage) for asphalt mixtures with variable packing. Measurement methods dry, SSD or dimensions (DIM) are given in parenthesis after the mixture type. VMA equals V_b+V_a, and V_a+V_b+V_s equals 100%.*

All measurements have precision and bias, and the question ultimately remains whether we can separate these from the true material variation caused by production. Quality assessment becomes complicated when testing methods with different precisions are mixed. Pellinen and Kutczek (2007) have studied this issue and they determined the allowable testing variation for the VMA to be ± 0.5%. Eq. (14) shows that the allowable testing variation for the VMA is a combination of testing variations of the three conventional laboratory tests for P_s, ρ_p and ρ_s. Figure 2 shows that for segregated pavement, the range of VMA was ca. 3%. Therefore, a production variation covering the physical segregation is within ± 1 % change of the VMA in the asphalt bulk property.

Asphalt density is thus needed to determine the weight-volume relationships and to calculate the volumetric quantities. To obtain an acceptable and sufficiently accurate reading for the air inside the specimen, several methods of obtaining the density or bulk specific gravity of a compacted sample are available.

3.3 Density measurement methods

There are a number of methods available to obtain the asphalt density and each one uses a slightly different way of determining the specimen volume, which may result in different density values as Figure 10 above indicates. In water displacement methods, which are based on the Archimedes principle, specimen volume is calculated by weighing the specimen in a water bath and out of the water bath. The difference in weights is then converted to the volume of the specimen. The three methods that are used in SFS-EN 12967-8 for obtaining the density of the compacted asphalt sample are a dry method (no water in sample) (A); a saturated surface

dry method (SSD) where water fills the asphalt air voids (B); a method based on the sample dimensions (D); and a method where the sample is sealed (C); for instance, wrapped with parafilm. The dry method is used for dense mixtures, such as MA and AC, while the SSD is used for the SMA mixtures. Dimensions are not typically used for other than the porous asphalt, to be precise, open graded asphalt, as the large voids cannot be measured with other methods. In addition, obtaining density with core dimensions is not considered sufficiently accurate a method for the AC and SMA. The Parafilm method is not typically used as it is considered to be tedious. There are no limitations for water absorption in SFS-EN 12967-8 method, but equivalent AASHTO T-166 standard states that water absorption should typically be below 2 percent. If more than 2 percent water by volume is absorbed by the sample, this method is not appropriate.

A correlation between different measurement methods can be developed, but it will be mixture dependent. Typically, differences increase with increasing air voids and specimen surface roughness. A measured volume can range from a solid volume (maximum density) to a volume with high surface roughness and texture. Figure 11 below shows a comparison between SSD and Parafilm methods for three Finnish surface mixtures SMA22, AB22 and SMA16 tested at Aalto University Road Laboratory. The measurements were taken according to SFS-EN 12967-8-B for SSD and SFS-EN 12967-8-D for Parafilm. Notably, most samples passed the tolerance limits of 6 % air, when measured with the SSD method, but failed the Parafilm method. This indicates that the SSD method does not capture the true air volume of the core. This problem is more pronounced for the SMA mixtures, which have a rough surface texture and a coarse aggregate skeleton. Water absorption ranged from 0.1 to 2.9 % by volume, average was 0.8 % and standard deviation was 0.7 %. The samples that passed the tolerance limit had less than 0.5 % absorbed water.

However, the same NDT electromagnetic method is applied for all mixtures, regardless of the magnitude of their porosity or surface texture. Therefore, the magnitudes of dielectric properties are directly comparable amongst different mixture types contradictory to the densities obtained with conventional methods.

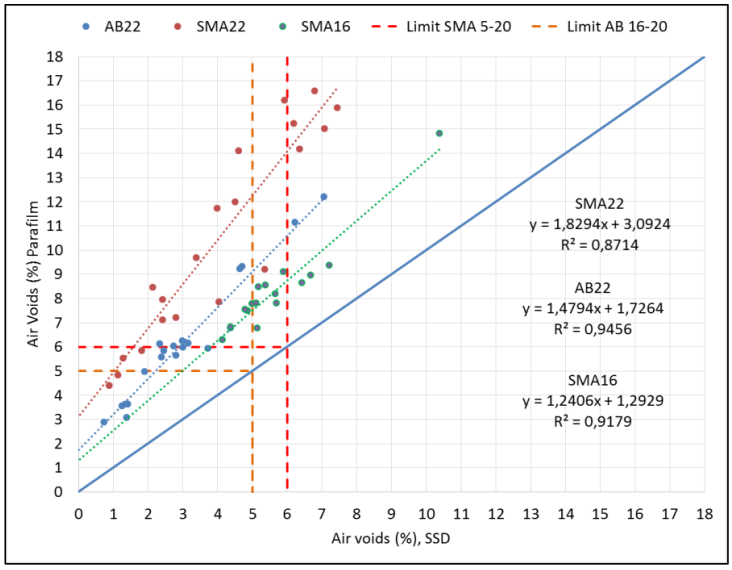

Figure 11. *Correlation of air voids obtained with SSD and Parafilm methods.*

4 REVIEW OF GPR CALIBRATION METHOD

4.1 Summary of research conducted 1996-1997

In 1996-1997, a study was carried out where the dielectric constant of asphalt pavements was investigated using laboratory and field measurements: *Päällystetutkatutkimukset* 1996-1997, Tiehallinto selvityksiä 4/1998. Based on this report, PANK specification PANK-4122 *Asfalttipäällysteen tyhjätila, päällystetutkamenetelmä*, was developed. Below is a brief review of the research based on current understanding about the capabilities of this technology.

The research team measured asphalt samples and slabs with different air void contents, mix designs and aggregates using a Percometer probe. An exponential regression model was fitted to the data, where y is the air void content and ε_r' is the measured dielectric value (see Figure 12 below).

$$y = 272.93 \exp(-1.3012 * \varepsilon_r') \quad (15)$$

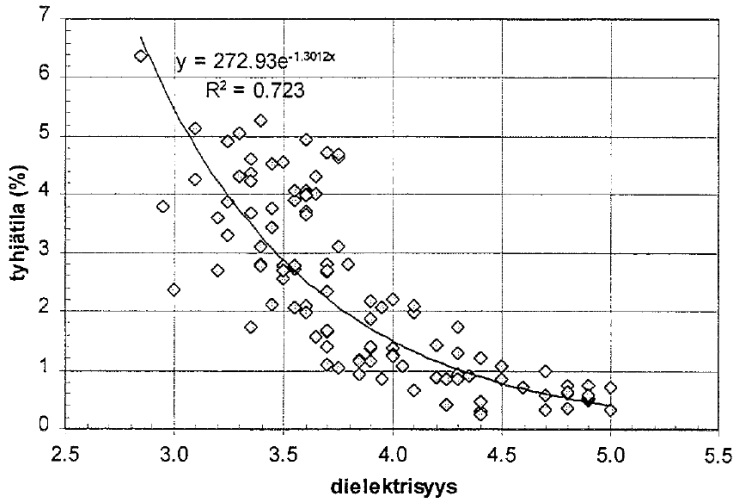

kiviaines	tyhjätila (%)		
	minimiarvo	keskiarvo	maksimiarvo
Latostenmaa, AB 16	0,3	0,9	2,1
Koskenkylä, SMA 18	1,3	3,6	6,4
Vaiskokuru, AB 16	0,4	2,5	4,9
Kuusajärvi, AB 25	0,9	2,4	5,1

Figure 12. *Laboratory measured (Percometer) relationship of air voids and dielectric constant (1996 study), Roimela, 1998.*

After developing the correlation equation, more measurements were conducted the following year using a new Percometer apparatus, see Figure 13. The new data did not match the previous data well. Researchers surmised that this was due to differences in aggregate dielectric properties and that shifting the data would correct this discrepancy.

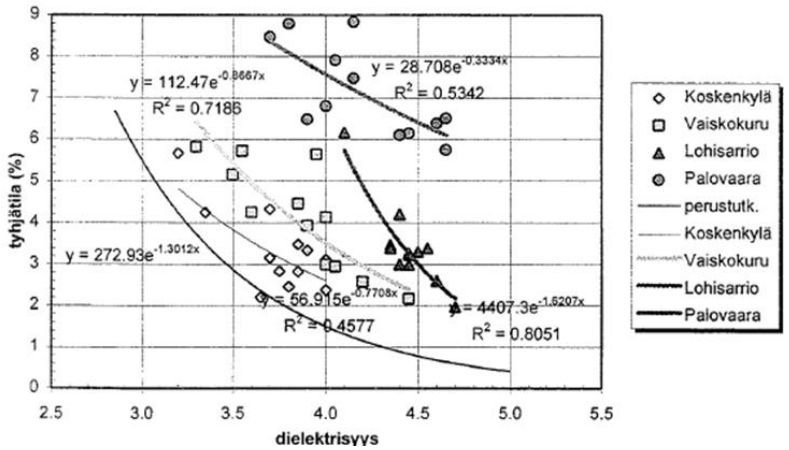

kiviaines	dielektrisyys			tyhjätila (%)		
	min	ka	maks	min	ka	maks
Koskenkylä, SMA 18	3,2	3,7	4,0	2,2	3,3	5,7
Lohisarrio, AB 16	4,1	4,4	4,7	2,0	3,4	6,2
Vaiskokuru, AB 16	3,3	3,9	4,5	2,2	4,1	5,8
Palovaara, emulsio	3,5	4,2	4,7	5,7	7,1	8,8

Figure 13. *Laboratory measured (Percometer) relationship of air voids and dielectric constant (1997 study), Roimela, 1998.*

A calibration factor *k* was introduced. Thus, the final calibration model that was adopted as the PANK specification became*:*

$$y = 272.93 \exp(-1.3012 * k * \varepsilon_r') \tag{16}$$

The next step in the research was to conduct field studies on nine roads which were measured using a GPR of SIR 10H with 1 GHz frequency (see Table 1 below). Cores were taken from eight to 12 places and the air void content was measured in the laboratory (see Table 2 below). The variation of GPR measurements ranged from 0.15 to 0.31. The largest variation was measured on the road Mt 9262 where the pavement had been rehabilitated using the bitumen stabilization method. The stationary measurements were conducted by stopping the vehicle and taking discrete measurements, which are presented in Table 2. The reported variation seems to be comparable to the variation in the continuous measurements.

The results of the air voids were back-calculated using the GPR. The air voids measured in the laboratory were plotted and a correlation of $R^2 = 0.92$ was calculated (see Figure 14). The GPR measurements were averaged over a distance of 3 meters to obtain the dielectric constant for each core location. As the back-calculated air void content is obtained by knowing the core air void content, this correlation does not represent an independent verification of the goodness of the prediction. It indicates the prediction capability of the calibration equation relative to the true air void content of the entire road pavement. As one core cannot possibly represent the entire pavement density variation, the true air void content will not be reliably determined by this method. Residuals around the regression equation suggest that there is ca. ± 2 percent variation in the average air void content.

Table 1. *Average dielectric value ε_r' and standard deviation for each test road, Roimela, 1998.*

kohde	jatkuva mittaus		Static Shot		sondi	
	ka	khajonta	ka	khajonta	ka	khajonta
Vt 1	4,38	0,22	4,56	0,15	-	-
Vt 4 Korvala	4,21	0,15	4,53	0,09	4,0	0,2
Vt 4 Vuojärvi	4,18	0,26	4,18	0,03	3,8	0,2
Vt 4 Vuotso	4,15	0,16	4,36	0,13	4,5	0,3
Vt 21	4,54	0,18	4,02	0,16	3,6	0,4
Mt 45	4,18	0,16	4,40	0,29	3,6	0,2
Mt 78	4,61	0,15	5,09	0,20	-	-
Mt 9262	3,38	0,31	-	-	-	-
Pt 11427	4,23	0,15	4,69	0,11	4,7	0,3

Table 2. *Information of test roads, reproduced from Roimela 1998.*

Road	Surface Mix	Quarry	Core air voids (%)		Thickness (mm)		Layer blow surface layer
			Avg.	St.De	Avg.	St.De	
Vt1 Espoo	SMA18	Koskenkylä	4.6	1.1	-	-	asphalt
Vt4 Korvala	AB16	Vaiskoru	2.9	0.7	-	-	asphalt
Vt4 Vuojärvi	AB16	Vaiskoru	4.0	0.6	95	10	asphalt
Vt4 Vuotso	AB16	Vaiskoru	3.7	0.7	44	10	crushed base
Vt21 Muonio	AB25	Kuusajärvi	1.6	0.4	56	6	crushed base
Mt 45 Tuusula	SMA 18	Koskenkylä	4.0	1.0	50	3	crushed base
Mt 78 Pudasjärvi	emuls.	Palovaara gravel	6.4	1.3	51	4	crushed base
Mt 9262 Keminmaa	PAB		9.4	1.2	49	16	bitumen stabilized
Pt 11427 Nurmijärvi	AB16	Latostenmaa gravel	1.9	0.8	-	-	

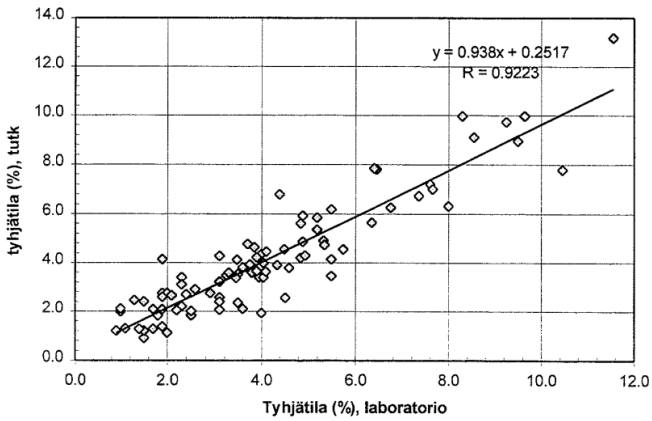

Figure 14. *Correlation between air voids of cores and air voids obtained from GPR, Roimela, 1998. Note that this correlation does not represent independent verification.*

4.2 PANK-4221 Calibration procedure

Based on Roimela's research, the calibration procedure was developed and adopted by PANK ry in 2000 for Finnish Asphalt Specifications. The PANK-4221 *Asfalttimassat ja -päällysteet, perusmenetelmät; Asfalttipäällysteen tyhjätila, päällystetutka-menetelmä* specification determines the calculation method for the air void content of the road by using dielectric values. The calibration process is divided into two methods: one for the conventional overlays and the "marker-method" for the REM and RC work.

For overlays with added amount of mixture > 80 kg /m^2, the method is as follows. First, the dielectric value is measured from the wheel path (typically right wheel path) with the air antennas 1 GHz, and the coordinates registered. Then the average of the dielectric value is computed. After that, two (2) representative locations of the road (length at least 5 km) matching the average dielectric value are chosen to take two replicate core samples, see Figure 15 below. The air void content of the cores is measured in the laboratory according to the EN-12697-8 standard. The value of the air voids is then applied to calculate the calibration factor *k* of the calibration equation. The calibration factor will be calculated for all core samples and the values averaged. This value can be applied to mixtures produced in the same asphalt plant using the same aggregates. The average calibration factor is then used to back-calculate the air voids of each measuring point. Finally, the quality control report presents the overall air void content of the road by averaging the back-calculated air voids values and calculating the standard deviation of the air void content. Dielectric values are measured ca. 10 cm apart and averaged for one-meter intervals. Each meter requires checking if the air voids are within the allowed limits. The report gives the number of measurements and the percentage of data points as being above the limit.

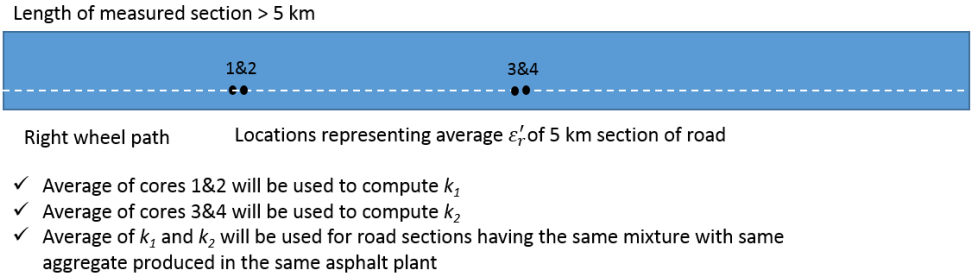

Figure 15. *Coring procedure for overlays in which amount of mixture is > 80 kg/m^2.*

In REM and RC work, the vehicle is stopped and the location is marked on the road where cores must be taken. The marker-method does not explicitly state the number of cores that must be taken or the number of locations that must be marked.

Measurements are not allowed when the road surface is wet, air temperature is less than 1°C or if the ground is frozen.

4.3 Observations

The 1996 relation between pavement voids and the dielectric constant was derived from samples made with four different aggregates. Although these aggregates are supposed to have

dielectric constants close to one another, this variation introduces an unnecessary unaccounted contribution to the pavement dielectric constant–and possibly a systematic error as different aggregates are not equally represented at different percentage values.

The 1996 relation between pavement air void content and dielectric constant has an exponential form. The data seems to motivate this, but no rationalization is given. If the exponential dependence is accurate, it should be possible to find a theoretical rationalization for it.

The problem of surface roughness affecting the Percometer measurements was acknowledged in the 1996 study. It may be that the probe reach (20 mm depth) was too limited in general to guarantee a truly representative measurement, though averaging several measurements somewhat allays this fear. The 1997 probe was apparently more reliable in this sense.

It seems that no significance has been attributed to the effect of frequency on the value of the dielectric constant. It is unclear whether differences between the Percometer and GPR could have been partly explained by their different frequencies (50 MHz vs 1 GHz).

Contrary to the Percometer that runs risk of measuring too locally, the reported GPR equipment measures ca. 0.3 m x 0.3 m area that is significantly larger than a drill core sample. Thus, the obtained volume percentage of voids values are necessarily averaged over a wider region. For example, if an estimate of statistical deviations (the percentage of pavement having voids outside the allowed tolerances) is desired, a careful scaling of results to match the drilled core sample sized averaging regions (as norms assume) is required.

Generally, the variances of averages decrease in inverse relation to the averaging count n. Thus, voids percentage standard deviation from 300 x 300 mm GPR measurements might be scaled to correspond to a 100 mm-diameter core sample standard deviation by formula

$$\sigma_{\text{scaled}} = (0{,}3^2 / (3{,}14 \cdot 0{,}05^2))^{1/2} \, \sigma_{\text{GPR}} \approx 3{,}386 \, \sigma_{\text{GPR}} \qquad (17)$$

The significance of correlation coefficients R^2 falling well below 0.9 on several of the assessments of the dependency in the report should be interpreted as follows: A variation of measurements A (e.g. the percentage of voids by dielectric constant) cannot completely explain the variation of measurements B (e.g. the percentage of voids from drill core sample). Scatter inherent in methods A and B may appear as 'noise' that a model cannot explain or predict. The presence of noise necessitates a careful analysis and large amounts of data to reduce the uncertainty related to the parameters of a regression model (filtering away the noise from those parameters). Though a large number of measurements may allow a near perfect determination of regression parameters, this is still incapable of reducing the effect of inherent noise on any particular measurement.

The average dielectric constant ε_r' is easily obtained, and a large number of measurements allows the accurate determination of its standard deviation (and if desired, higher statistical moments to achieve an even more accurate description of the distribution of the dielectric constant). Paradoxically, even if the distribution can be obtained arbitrarily accurately, it is impossible to tell from measured data where extreme values occur. Due to the large averaging region size in a GPR measurement, any local change in the dielectric constant is masked or diluted and may be indistinguishable from measurement noise.

It is conceivable that a more reliable wave propagation model can be developed than the apparently rather (theoretically) weakly motivated dependency between voids and the dielectric constant as presented in the 1996-1997 report. If future work involves higher frequency GPRs, there may be more need for understanding the physics of wave propagation as the wavelength approaches the size scale of pavement granularity.

Figure 16 illustrates the formulation between the volume of air and the dielectric constant of a material based on a linear relationship and the well-known theoretical mixing models of CRIM, LLL and Maxwell Garnett. The ε_r' of material without air is 6 in the figure. At 100 percent air voids, the ε_r' should be 1 as there is only air in the total volume. In practice, a loose or not compacted asphalt mixture will have volume of voids ca. 40% and after paver compaction and before roller passes, there may be 10 to 20 % of voids based on the air-water measurement method.

At zero air, the dielectric properties of the mixture are dependent on the dielectric properties of its components. Therefore, the dielectric constant of dry mixture should not exceed the dielectric constant of a mixture at its maximum density (G_{mm}). If the mixture exceeds this value, it indicates that the mixture is not dry and there is water in the pore volume.

For comparison, Figure 16 below presents the PANK calibration model with k =1 and k=0,676, which represents an average k of 2009 REM work measurements, discussed more in Section 4.4. As the figure shows, the exponential PANK model form is physically incorrect. Although the adjusted model (k = 0,676) reduces underprediction, the model form is still erroneous. This is a result of misleading experimental observations based on weaknesses associated with the measurement of air void content of cores and the dielectric constant measured in the laboratory and in the field.

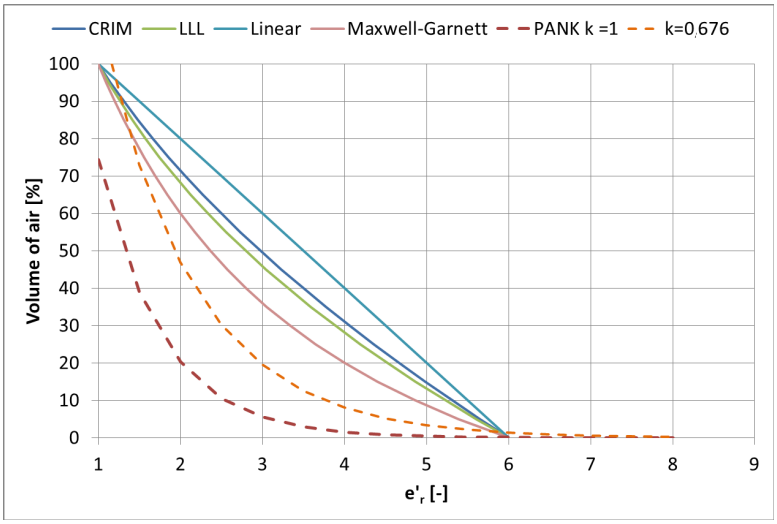

Figure 16. *Air-mixture relationships based on known mixing models and PANK calibration equation.*

4.4 Review of QC measurements with GPR for 2009 REM contracts

This section discusses the preliminary investigation of GPR quality control measurements retrieved from 2009 quality control records of the Uusimaa, Häme and Turku districts. The quality control reports of 49 resurfaced road sections were examined in order to evaluate the statistical variation of GPR based air voids measurement. All roads were resurfaced using the REM-method. The quality control data included the following information:

- Road section
- Length (m)
- Lab measured air voids of a core sample (%)
- Dielectric constant around core samples
- Calibration factor
- Average of air voids (%) based on GPR measurements
- Standard deviation of air voids (%) based on GPR measurements
- Length of pavements exceeding air voids limits

A summary of air voids measurement results is shown in Table 3. For 49 measured sections, the average air void content was 2.8%, which indicates very good pavement compaction. Similarly, the very low standard deviation of 0.47 suggests extremely good and homogeneous compaction work. The average dielectric constant value is 5.5 which is ca. 1 unit higher than the GPR field measurement values reported in Roimela's study (see Table 1).

Table 3. *Summary statistics for the rehabilitated roads based on GPR measurements.*

	Air void content (%)		Calibration factor *k*		ε_r'	
n	Avg.	St.Dev.	Avg.	St.Dev.	Avg.	St.Dev.
49	2.8	0.47	0.676	0.103	5,.5	0.78

4.4.1 *Dielectric values vs. air voids of rehabilitated pavements*

Figure 17 shows GPR measured dielectric values and the lab measured air voids. A plot of the calibration factor curve is also presented for k values of 1, which represent the original laboratory results and $k = 0.676$, which is the average of the 49 road sections studied. Error bars shown in the figure represent a variation of ± 2 times standard deviation. Standard deviations were obtained from the VTT model correlating the average air void content to the standard deviation of measurements given in Figure 18.

The results can be compared with Roimela's results as shown in Figure 12. The values are even more scattered than in the original research. As these values are used for calibration, more uniform results should be required. Figure 17 shows that the SMA mixtures deviate most from the calibration equation and they have the highest variation. The majority of SMA pavements had dielectric values above the grand average ε_r' of 5.5.

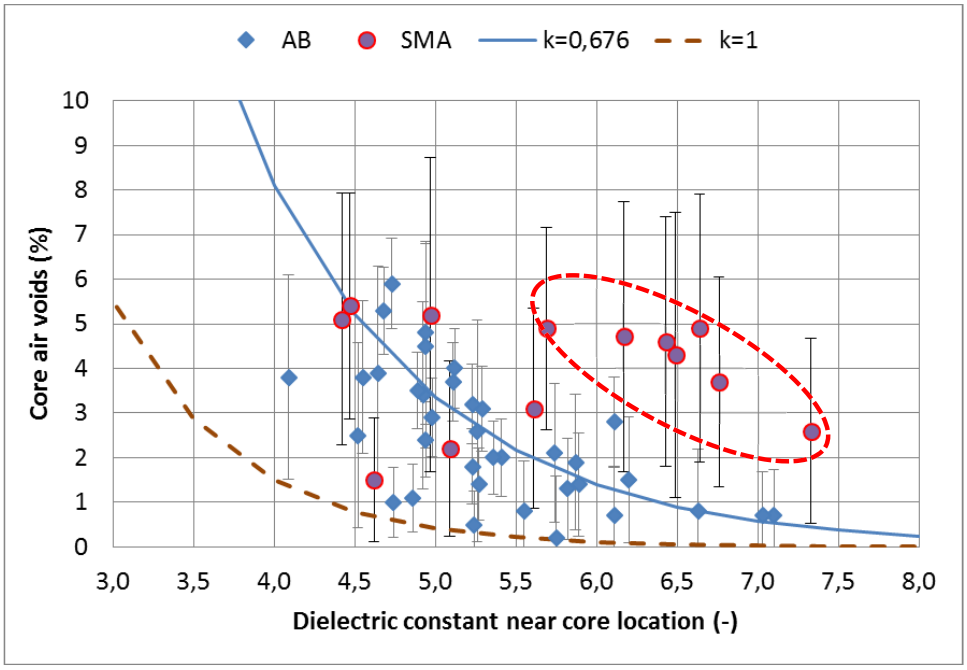

Figure 17. *Average dielectric values and air void content of calibration cores.*

A weak exponential correlation $R^2 = 0.43$ can be found by excluding the points inside the red ellipse. However, a large variation with lower dielectric values remains. For example, with a dielectric value of 4.9 ± 0.07, air voids between 1.1 % and 5.2 % were measured from the core samples.

4.4.2 *Standard Deviation*

The standard deviations of the air void content measurements were compared with the results from the literature. Hyyppä (2000) analyzed a very large database of road QC/QA measurements in his dissertation. The VTT Road Laboratory collected this database during the years 1981-1990 by measuring 21 756 core samples from 627 construction sites. Hyyppä gives a model for the density variation as a function of air void content, which is reproduced in Figure 18. The figure shows that the standard deviations for the air void content, derived from GPR measurements using the PANK calibration method, are generally smaller than the conventional laboratory air-water measurements.

It can be observed that the data is not homoscedastic as the variance increases with higher average air void contents. Therefore, the quality control data was divided into two parts, according to pavement types. Figure 19 shows the results of SMA pavements, and Figure 20 shows the results from AB pavements.

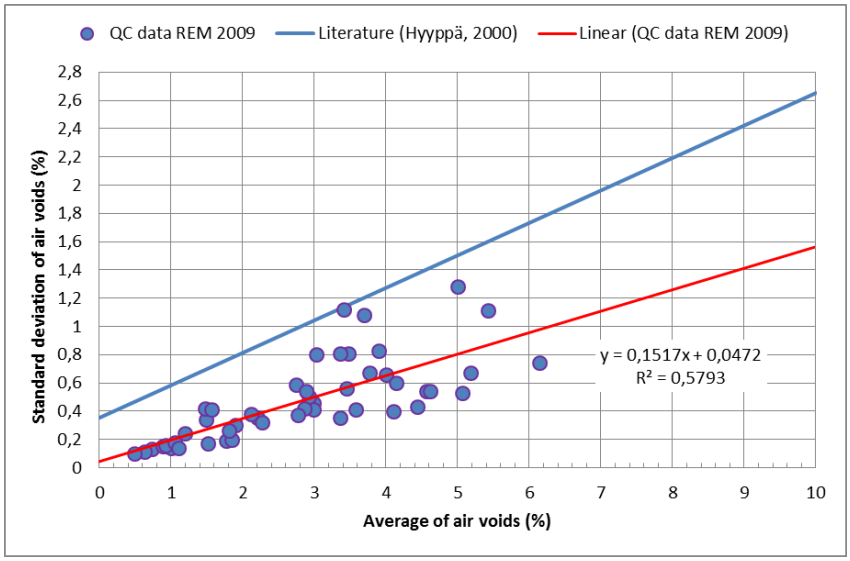

Figure 18. *Average air voids and standard deviation of the quality control data. The blue line (y=0,23x+0,35) corresponds to the linear data fit (R^2=0,984) of the results from Hyyppä (2000).*

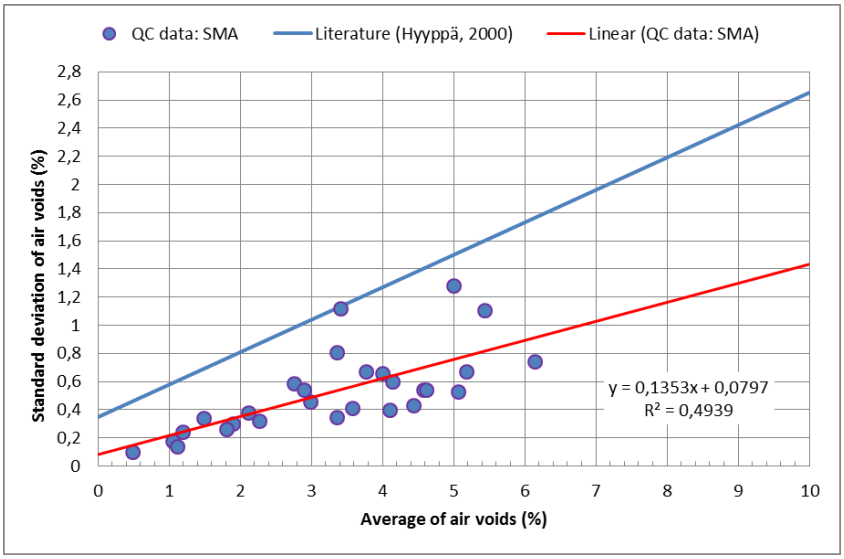

Figure 19. *Average air voids and standard deviation of the quality control data, SMA surfaces only.*

The coefficient of determination (R^2) for the fitted line in Figure 19 is 0.49. The slope of the line (0.1353) is smaller than for the entire dataset suggesting more uniform compaction work as air voids increase. However, this is not the case, the reason for declining variation is in the problem of measuring the air void content of SMA cores using a representative method (see Figure 11).

Residuals for AB surfaces are considerably smaller (R^2 = 0.74) than for the SMA surfaces. Moreover, the slope of the line (0.2257) seems to be very close to destructive QC control data (slope of 0.23). However, at zero air voids, content variation becomes negative, which is not physically possible. Overall, this indicates that the measured trends are similar due to the calibration process, but there is a systematic bias in the back-calculated air void content values produced by the GPR method.

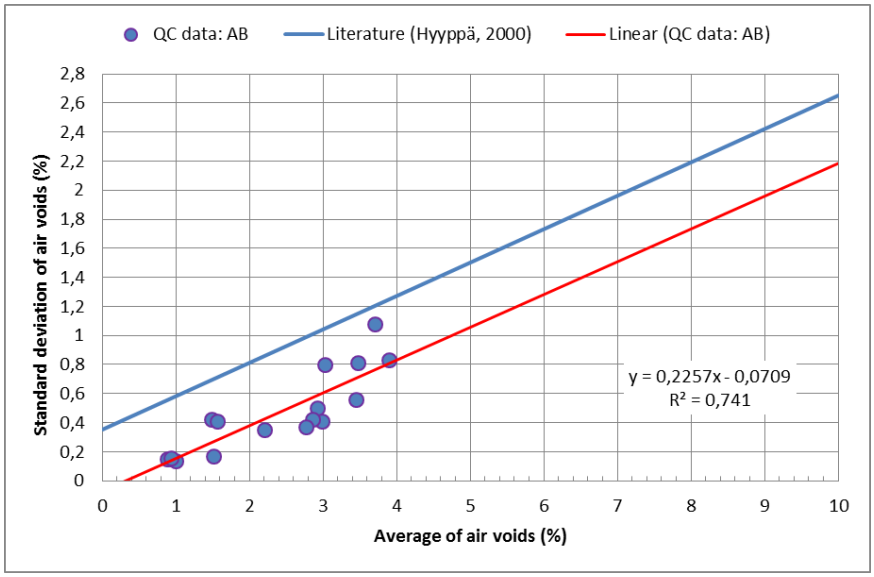

Figure 20. *Average air voids and standard deviation of the quality control data, AB surfaces only.*

4.4.3 *Calibration Factor*

Most of the sections had only one calibration sample, as the length of the section was below 10 000 meters. However, the sections with a length of more than 10 000 meters, had at least two calibration samples. In those cases, the calibration factor has been determined by calculating the factor for each sample and then using the average value for the whole section. We estimated the sensitivity of the calibration factor (*k)* by calculating its minimum and maximum values. The results can be seen in Table 4.

Table 4. *Calculated k-values using two core samples. The average k-value was used in QC.*

	Road A	Road B	Road C	Road D	Road E	Road F	Road G
Lower k	0.465	0.706	0.722	0.639	0.629	0.645	0.653
Average k	0.478	0.728	0.763	0.659	0.713	0.661	0.677
Upper k	0.491	0.750	0.803	0.680	0.798	0.676	0.701

According to Table 4, by adjusting the *k*-value by 0.01, the average of air voids will change by 1%. Therefore, using only one *k*-value for long sections or the same *k*-value for both directions, the calculated air voids results may significantly distort.

4.4.4 *Penalties for exceeding the limits*

The total length of the pavements exceeding the upper threshold value of air voids are presented in Table 5. These results are collected from the QC reports.

Table 5. *Amount of penalties caused by too high air voids values.*

	Häme	Turku	Uusimaa
Length of road having too high air voids (m)	3212	6355	2006
Total amount of penalties (€)	20 866.95	3 846.54	0
Amount per meter (€/m)	6.5	0.6	0

In the Uusimaa area, more than 2000 meters of pavements were recorded as having overly high air voids. Nevertheless, no penalties were issued to the contractors. As no additional information was available, we suggest that this issue be investigated more closely in the future.

4.4.5 *Back-calculation of aggregate dielectric constant*

By utilizing the ALL model (Eq. 13), it was possible to back-calculate the aggregate ε_r' for most of the roads in the database. Back-calculated rock aggregate dielectric constant values ranged from 6.96 to 9.99, the average being 7.91 with the standard deviation of 0.76. These values are too high for the typical aggregates used in Finland for the asphalt production. This will be discussed more in Section 5.3.1.

4.4.6 *Summary of the QC measurement review*

The following conclusions can be drawn from the review of quality control repots:

- There is no clear linear or nonlinear correlation between the dielectric values and the air voids of core samples.
- The standard deviation of GPR based air voids measurements are significantly smaller than the conventional laboratory measured air voids.
- More attention should be paid to determining the calibration factor *k* from core samples in long pavement sections.
- Penalties defined for contractors are not in line with the amount of sections exceeding the threshold values of air voids.
- However, it is not known what influence, if any, the REM rehabilitation method had on presented results. There is no clear joint between the top layer and the asphalt layer below; therefore, it is unclear how the radar signal would separate the top layer from the lower layers.

4.5 Review of the Mara Nord Project

During 2010-2012, the Mara Nord project was conducted between the Finnish, Swedish and Norwegian transport administrations, consultant companies and GPR manufacturers (Narbro et al, 2012). One of the project objectives was to create common Nordic recommendations of GPR

services for road surveys. The project was divided into work packages and the WP5 concentrated on improving the reliability of the existing air void content determination method. During this project, some laboratory and field experiments were performed which were designed to increase the accuracy of the current regression model (Peisa and Poikajärvi, 2012). Laboratory experiments were conducted manufacturing a large asphalt slab with the thickness of 50 mm and measuring it in the laboratory with actual GPR antennas.

However, it was impossible to find a reliable regression model between asphalt void content and the dielectric value based on the experiments. One of the reasons for this might be that the sample thickness of approximately 50 mm was too thin; therefore, the reflection from the sample bottom interfered with the surface reflection. Furthermore, the sample plate compaction was not constant around the sample plate.

The field experiment in WP 5 was conducted by driving over the test section with different vehicles twice and then comparing results. The field experiments showed that the repeatability and reproducibility of the air void method are good although some exceptions were observed. However, the reliability of the method is questionable when different calibration cores are used. It was also observed that for some data sets the variation of air voids does not follow the current model despite the adjustment of the calibration factor. Therefore, a new method, wavelet analysis, was introduced to evaluate the homogeneity of the pavement, but the method was not validated in the Mara Nord project.

4.6 Conclusions

Based on the observations above, the following conclusions can be drawn:

- The original PANK calibration regression model form is incorrect due to experimental errors associated with both the core air void content and the GPR measurements.
- Calibration factor *k* artificially reduces the true air void content variation by truncating a variation of permittivity measurements.
- The air-water method of obtaining air void content for SMA mixtures fails to measure large voids in the surface of pavement and its capacity to hold water.
- It is hypothesized that the elevated ε_r' values are not caused by a variation in aggregate dielectric values but moisture in the unbound and asphalt layers.
- A severe problem with currently available commercial GPR equipment (at 1-2 GHz) is the inadequate depth resolution, which unavoidably causes erroneous ε_r' values due to reflections from successive layer interfaces. In fact, without some a priori information or an estimate of top layer thickness or dielectric constant ε_r', the GPR technique easily fails to provide any meaningful data.

5 FIELD GPR MEASUREMENTS AND SAMPLING

5.1 Test roads and GPR measurements

During the summer of 2013, field experiments were conducted near Tampere on two roads: Vt3 (Location 1) in the Pirkanmaa area, and Vt12 (Location 2), also in the Pirkanmaa area. Table 6 summarizes the locations, measurements dates, numbers of data points and type of measurement. Figure 21 visually dmeonstrates the way the GPR measurements were conducted relative to core locations.

Table 6. *Summary of core locations and measurements in 2013.*

Road	Coordinates	Date 2013	Type of	measured distance, m	No. of data points
Vt3	6818486 N, 324209 E	17.07.	Continuous, right wheel path, centre	2 x 9183	2x 9183
		20.08.	Continuous, right wheel path, centre	2 x 4350	2x 4350
		20.08.	Stationary on coring locations	4 x 0.3	4x100
		26.08.	Continuous, right wheel path, centre	2 x 4350	2x 4350
		30.09	Continuous, right wheel path, centre	2 x 4350	2x 4350
Vt12	6822254 N, 319144 E	11.11.	Continuous, right wheel path, centre	2x 3573	2x 3573
		11.11.	Stationary on coring locations	7x0.3	7x1350

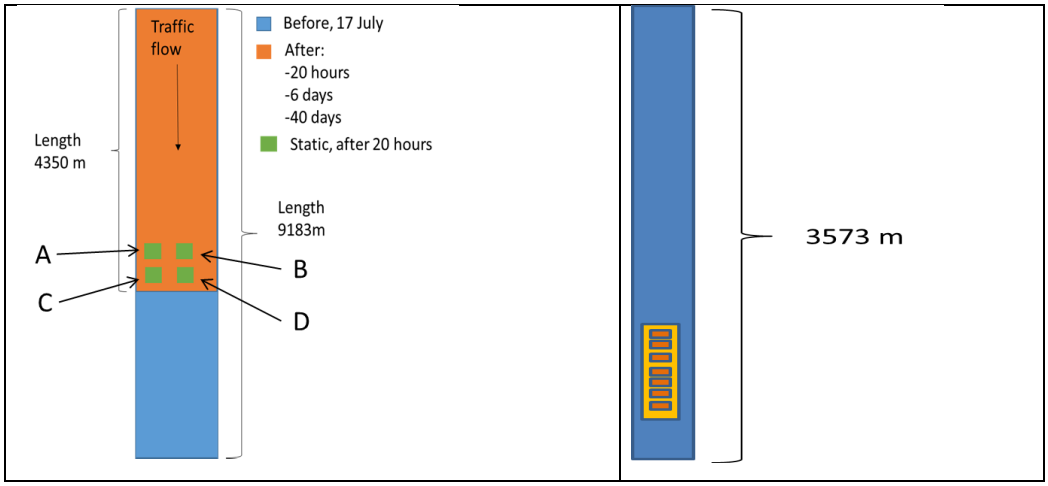

Figure 21. *Illustration of GPR measurements. Vt3 left and vt12 right. Both roads are in the direction of 221 in the Road Registry.*

Both roads were paved with the same SMA16 mixture. Vt3 was overlaid with a fresh mixture to produce a ca. 40 mm thick new pavement layer (this method is called “massapintaus” in Finnish). Vt3 was a multistage construction project and the SMA16 layer was the required wearing course structural layer to complete the construction. Vt3 pavement structure is shown in Appendix A. The asphalt was produced in the asphalt plant located in Syrjänsalo. The distance between the asphalt plant and sampling location (1) in Vt3 is approximately 26 km, and in travel time, around 22 minutes. At Vt12, the old road surface was milled and removed and then filled with a new asphalt mixture. The distance to location (2) in Vt12 is 18 km and travel time 18 minutes. Figure 22 shows the locations of the asphalt plant and the Mäyry quarry.

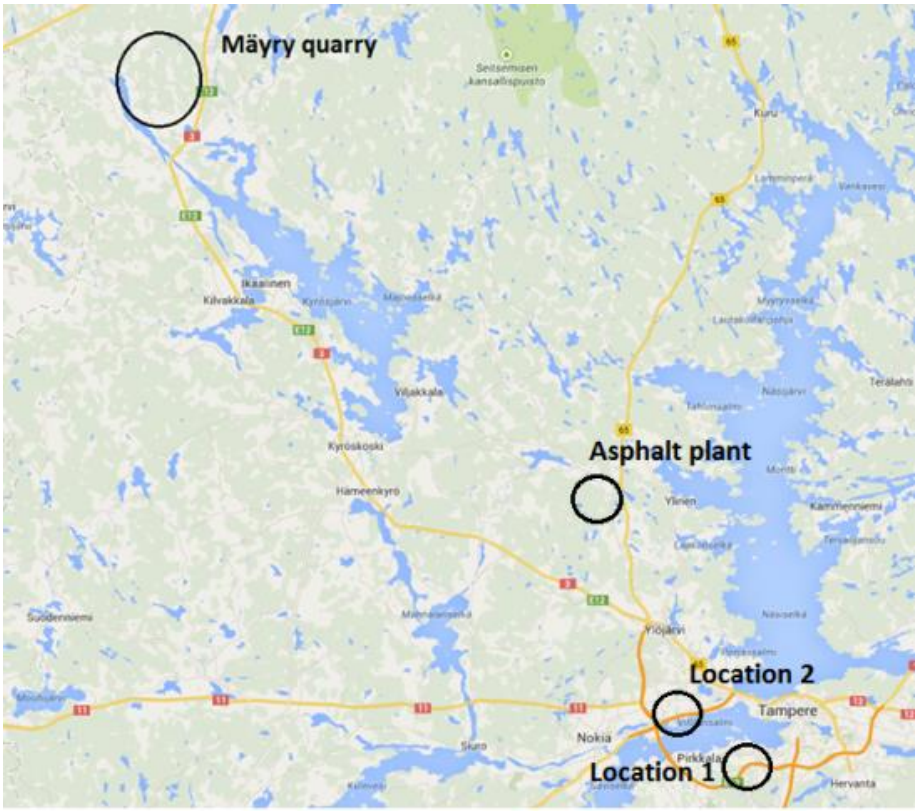

Figure 22. *Locations of asphalt plant, sampling and Mäyry quarry. (Map data ©2015 Google)*

For both roads, the aggregates used in the driving lane (Lane 1) are different from the passing lane (Lane 2). The aggregates for Lane 1 come from the Mäyry quarry; for Lane 2, aggregates come from the same quarry where the asphalt plant is located. Lane 2 aggregates were classified as AN10 against resistance to wear by an abrasion from studded tires (SFS-EN 1097-9). This category is not sufficiently adequate to be used in a driving lane, but can be used in a passing lane. Aggregates from Mäyry have the classification of AN7, which allows them to be used in the driving lane.

The weather conditions for the dates of the construction until the last GPR measurement were obtained from the Operational climate service. The data includes the average temperatures, maximum and minimum by day and the rainfall. During construction of Location 1 (Vt3), the weather was warm and dry. The weather during construction of Location 2 (Vt12) was also warm and dry. Figure 23 shows the rain history and Figure 24 temperatures.

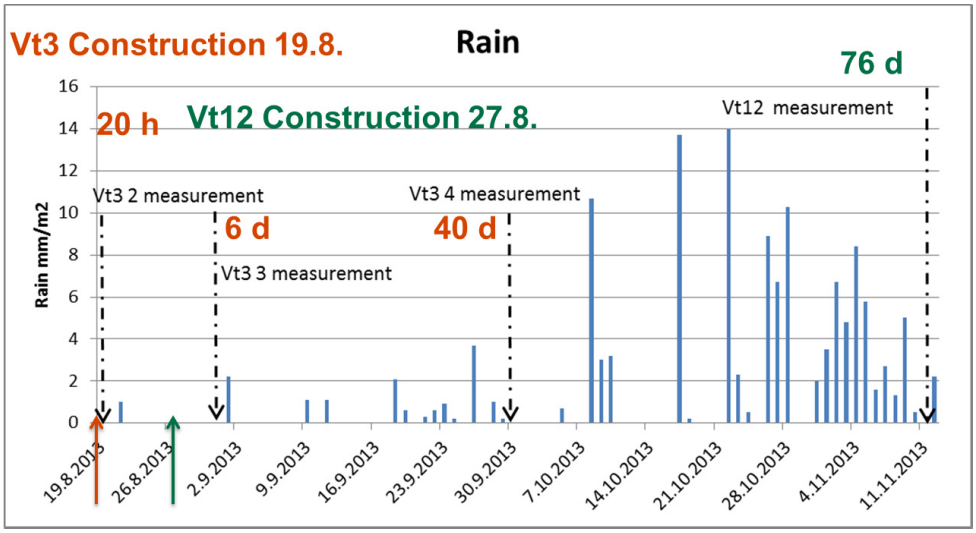

Figure 23. *Weather information: rainfall.*

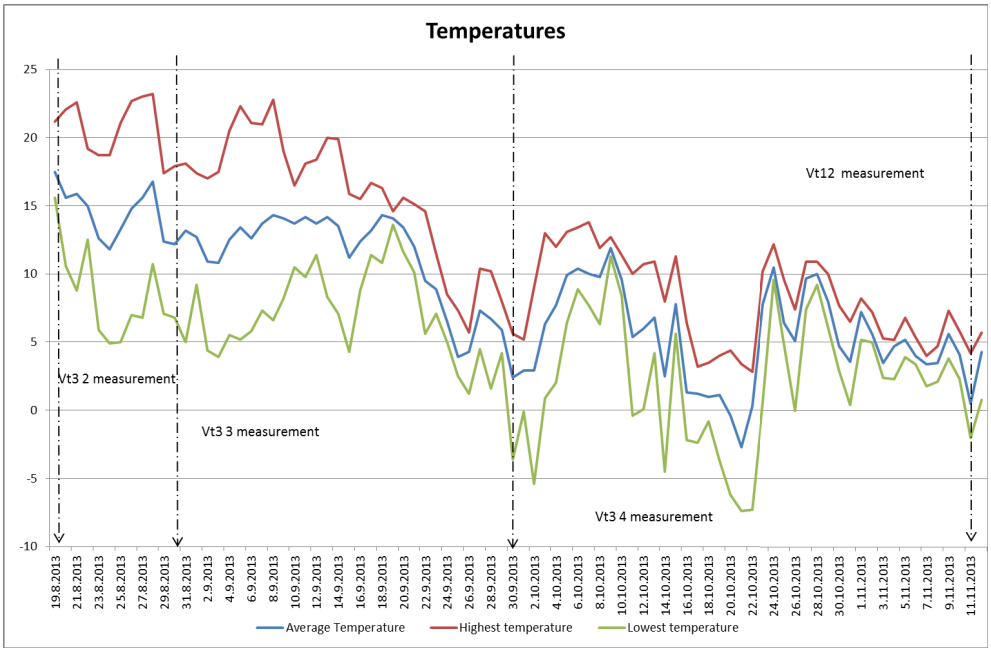

Figure 24. *Weather information: temperatures.*

The dielectric permittivity of the pavement was measured using 2.2 GHz GPR. Location 1 (Vt3) was measured four times. Measurements were taken from the right wheel path and the center space between the wheel paths. The first measurement was carried out 17th July, before paving work on the road started, covering 9183 meters of road. The second measurement was taken 20th August; around 20 hours after the compaction of Location 1 covering 4350 meters of road (see Figure 21). That measurement included the continuous measurements and four stationary measurements on top of the four precise areas, from which samples were taken later. Figure

25a shows one of the stationary measurements. Then the shorter section of the road was measured for the third time six days later on the 26th August. The last measurement was conducted one month later on 30th September. Location 2 (Vt12) was measured on 11th November, two months after construction. In that location, the measurements were taken using the continuous method for the right wheel path, starting one kilometer before the location and ending one kilometer after (see Figure 21 below). Stationary measurements were taken from seven spots in the road. Figure 25b shows the actual locations of seven stationary measurements.

(a) (b)

Figure 25. *(a) Stationary GPR measurements, left Vt 3 (Location 1) and (b) Vt12 (Location 2).*

5.2 Taking slabs and cores from the roads

The original plan was to take four slabs and 24 cores of Ø 150 mm from the surface layer. However, due to difficulties in taking slabs, this plan was not successful. The following section describes all the trials and work that were conducted to collect cores and asphalt slabs.

5.2.1 *Sampling on Vt3*

Sampling started on 19th August from Vt3; it was decided to use a sand layer placed on the road surface before the asphalt would be laid down, as is shown in Figure 26a. The aim was for the sand to prevent the top layer from being glued to the surface below, then a slab would be cut out of the pavement using a portable Husqvarna floor saw as shown in Figure 26b.

The sand size used was 0/2 mm. Two layers were placed in 6818486 N, 324209 E and 6818483 N, 324206 E according to ETRS-TM 35FIN coordinate system. The sand covered the width of the lane as is shown in Figure 27a. The trucks and the paver went over the sand layer without removing too much, Figure 27b.

(a) (b)

Figure 26. *Layer of sand on top of the bitumen glue and right Husqvarna floor saw.*

(a) (b)

Figure 27. (*a) Truck drives over the sprinkled sand layer; b) Sand layer after the caterpillar wheel of the paver.*

Next day, after the road had been measured by GPR, an attempt was made to take the slabs from the road. Unfortunately, it was impossible. The top layer was glued to the lower layer and the slab could not be cut out. Figure 28 shows the attempt to remove the mixture, in order to enable properly patching of the location.

Figure 28. *Cuts made in the slab to remove the mixture.*

On 21st August, cores of 150 mm in diameter were taken from the areas measured by the GPR. Figure 29a show the core layout of the sample coring and Figure 29b show the actual coring locations. Sample 19 was destroyed during the extraction process. The cores inside the same square area are only separated by few centimeters, as shown in Figure 30.

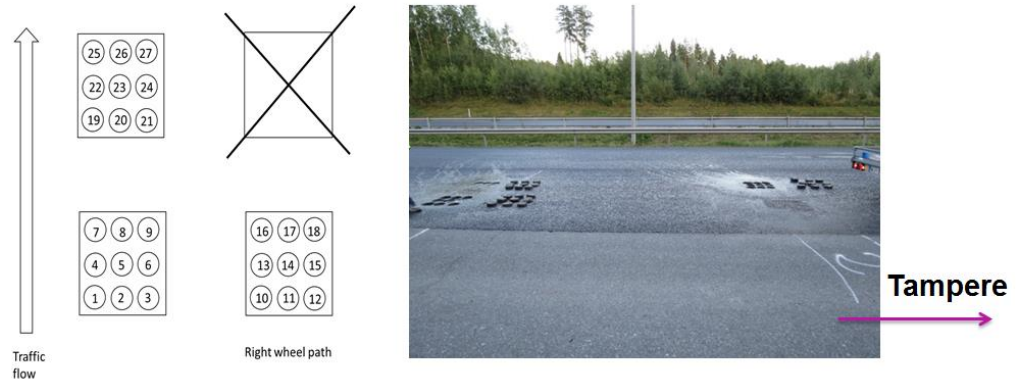

(a) (b)

Figure 29. a) *cores from 1 to 27; b) Location 1 (Vt3) after sampling. Longitudinal distance between core sets is 10 m and transverse distance is 2 m.*

After the failure to acquire slabs from Location 1, some trials were conducted at the Road Laboratory backyard with different materials apart from sand, see Figure 30. None of the attempts produced satisfactory results. Finally, it was decided to use a wood cover with silicone paper and apply grease on top of a thin layer of calcium oxide. The wood would be nailed to the pavement to prevent it from moving during compaction, see Figure 30b.

(a) (b)

Figure 30. *a) Trials with calcium oxide; b) Wood plate nailed to the pavement.*

5.2.2 *Sampling on Vt12*

The sampling took place 27th August and the original plan was to use the same positions to take four slabs, as was employed in Vt3 for the location 1; two slabs from the right wheel path and two slabs from the center. However, this plan had to be modified due to the paver operator's concerns about not being able to level the paver. Then it was decided to place the wooden plates on a row in the middle of the lane, see Figure 31.

Figure 31. *Placing more grease on the wooden plates.*

During compaction, it became evident that there was not enough mixture on top of the wooden plates for proper roller compaction (see Figure 32a) and more mixture had to be added to the plate area (Figure 32b).

(a) (b)

Figure 32. *a) Overly thin layer of mixture on top of the wooden plates. b) More mixture had to be added.*

It seems that during compaction the wooden plates moved slightly up and down. This caused poor roller compaction and thinner slabs than were intended. In addition, the mixture was not

homogeneous, see Figure 33a. On 2nd September, we returned to extract the slabs, but two of the slabs were already damaged, see Figure 33b.

(a) (b)

Figure 33. *a) Location of the wooden pates is clearly visible. b) Pavement was deteriorated by traffic loading on locations for slabs 2 and 3 and they were already damaged.*

It was possible to extract only Slab 1 and 4. 10 cores of 100 mm in diameter were drilled to check the homogeneity of the mixture around the slabs. The actual sampling map is shown in Figure 34a. Figure 34b shows the road after sampling.

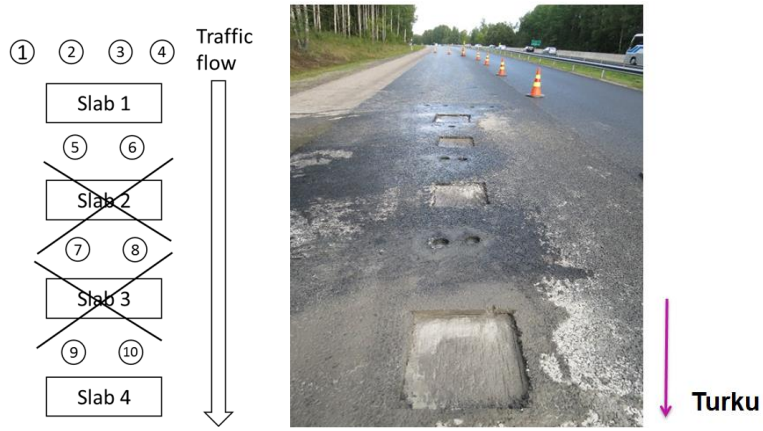

(a) (b)

Figure 34. *a) Actual sampling map. b) Road after sampling.*

Slab 1 broke during extraction, but the slab dimensions were still acceptable being ca. 0.4 x 0.4 x 0.028 m as the plan was to take 0.5 x 0.5 m slabs. Slab 4 dimensions were ca. 0.5 x 0.5 x 0.032 m and it was in better condition for further studies, see Figure 35a and b.

(a) (b)

Figure 35. *Vt12 sampling: pavement slab 1 and b) slab 4.*

5.2.3 *Sampling of mixture raw materials*

The raw materials were collected from the quarry and the asphalt plant. On 20th August, Lane 1 asphalt mixture was collected from the paver. The next day, 21st August, cold feed aggregate blend without fibers around 160 kg was collected (see Figure 36 below).

(a) (b)

Figure 36. *a) Blended aggregate without bitumen and fibers. b) Rocks collected from Mäyry quarry*

On 2nd September, bitumen, fibers, limestone filler and two buckets of asphalt mixture (Lanes 1 and 2) were collected for further studies. Lane 2 mixture would be used for verification purposes. On the same day, we also collected around 50 kg of rocks from the Mäyry quarry, see Figure 36. Table 7 summarizes all the collected materials.

Table 7. *Summary of sampled materials*.

Material type	Aggregate origin / Material origin	Road location	Lane	Mass (kg)	Date
SMA16	Syrjäsalo	Tampere Vt3	2, left lane	49	18.8.2013
SMA16	Mäyry	Tampere Vt3	1, right lane	21	19.8.2013
SMA16	Mäyry	Tampere Vt3	1, right lane	45	19.8.2013
Bitumen 70/100	Nynas	Tampere Vt3		7	2.9.2013
SMA16	Syrjäsalo	Tampere Vt3	2, left lane	5	20.8.2013
SMA16	Mäyry	Tampere Vt3	1, right lane	5	19.8.2013
Limestone filler	Vampula	Tampere Vt3		7	2.9.2013
Fiber	Ylisvilla	Tampere Vt3		1.5	2.9.2013
Mix blend	Mäyry	Tampere Vt3	1, right lane	160	21.8.2013
Rocks	Mäyry			50	2.9.2013
Asphalt slab 1 to 4	Mäyry	Vt12	1, right lane		2.9.2013
10 cores 100 mm	Mäyry	Vt12	1, right lane		2.9.2013
27 cores 150 mm	Mäyry	Vt3	1, right lane		21.8.2013

The contractor provided the construction records, which included mix designs, quality control gradation curves, bitumen content, type of bitumen and the air voids quality control reports. In addition, the theoretical maximum density was also provided, not to mention the design bulk density, the expected air voids, the voids in mineral aggregate (VMA) and the voids fill with bitumen (VFB). Finally, the records included the results of the Prall test (SFS-EN 12697-16 A) and the water sensitivity of bituminous specimens test (SFS-EN 12697-12 A).

6 RESULTS OF THE LABORATORY EXPERIMENTS

6.1 Experiment set-up for the RVE experiment (Vt3)

To set up the experiment for the Representative Volume Element (RVE) of asphalt, a quantity designated as the measured volume element (MVE) was defined. The MVE for the field measurements was dictated by the GPR measuring system and coring was done using a 150 mm core drill pit. Figure 37 below illustrates six MVEs determined for this study, the details of which are provided in Table 8. The largest MVE of 1.34E-02 m^3 was for the current GPR measurement method, and the smallest MVE of 1.41E-05 m^3 was for the VNA point measurements. The VNA point measurement MVE is 98% smaller than the core MVE. The layer thickness needed in the calculations was estimated from the cores obtained.

Table 8. *Description of MVEs in this study.*

MVE	Description	Area, m^2	Height, m	MVE, m^3	MVE Ratios	
1	Continuous GPR 0.3 x 1 m	3.00E-01	0.04474	1.34E-02	-	-
2	Stationary GPR 0.3 x 0.3 m	9.00E-02	0.04474	4.03E-03	MVE2/MVE1	0.30
3	Area of 9 cores 0.5 x 0.5 m	2.50E-01	0.04474	1.12E-02	MVE3/MVE1	0.83
4	One core ϕ 150 mm	1.77E-02	0.04474	7.91E-04	MVE4/MVE1	0.06
5	VNA scanning 75 x 75 mm	2.50E-03	0.04474	1.12E-04	MVE5/MVE4	0.32
6	VNA point 20 x 20 mm	3.14E-04	0.04474	1.41E-05	MVE6/MVE4	0.02

The GPR used in the experiment was 2.2 GHz impulse radar with horn antennas. Measurements were taken from the right wheel path and from the centerline of the road. The stationary measurements were conducted by stopping the vehicle and taking scans from the same spot continuously for 100 times. Continuous measurements were taken by measuring a stretch of the road and the data records were matched with the help of GPS coordinates. During paving work and measurements, the weather was warm and dry.

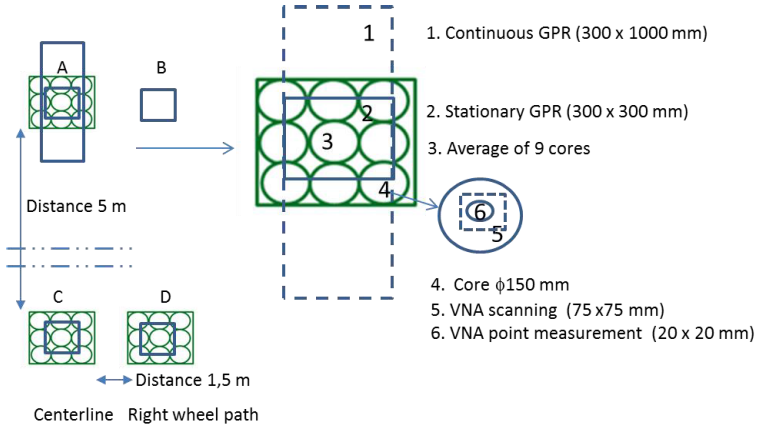

Figure 37. *Schematic presentation of MVE for GPR and coring. Not to scale.*

A total of 27 cores of 150 mm diameter were extracted from the road. The coring area was ca. 0.5 x 0.5 meters and the stationary measurements were matched on that same spot. The distance between cores in each test spot was kept within a few centimeters to minimize the material variation due to physical and thermal segregation. The distance between locations A - B and C - D was ca. 5 meters. Location B was not cored. Core no. 19 broke during coring.

6.2 Results of the RVE experiment and discussion

6.2.1 *GPR Measurements*

Table 9 summarizes the results of the stationary and continuous measurements. For the stationary measurement, areas B and D have the same ε_r' while area A and B are statistically significantly different.

Table 9. *Summary of GPR measurements on 20 h after construction (17.07.2013).*

Location		Stationary 300x300 mm including 100 x avg. of 10 scans		Continuous 0.3 x 1 m average of 10 scans	
		Avg. ε_r'	St.dev. ε_r'	Avg. ε_r'	St.dev. ε_r'
A	Centerline	5.38	0.04	5.0	0.1
B	Wheel path	5.43	0.06	5.3	0.1
C	Centerline	5.66	0.05	5.1	0.1
D	Wheel path	5.43	0.06	5.4	0.1

6.2.2 *Laboratory measured air void content*

Table 10 to 12 summarize laboratory measurements for cores. Pavement density, in other words, bulk specific gravity G_{mb} was measured using the SSD method and dimensions according to SFS-EN 12967-8. The maximum density (or the maximum specific gravity) of the mixture is G_{mm} and V_a is the voids in total mix or the air voids of specimen.

Table 10. *Bulk specific gravies of cores for location A in the centerline of the road.*

Location A (center line)					
Id	G_{mb} (DIM)	G_{mb} (SSD)	G_{mm}	V_a % (DIM)	V_a % (SSD)
19	-	-	-	-	-
20	2.370	2.494	2.538	6.6	1.7
21	2.349	2.489	2.536	7.4	1.9
22	2.261	2.484	2.538	10.9	2.1
23	2.275	2.491	2.544	10.5	2.1
24	2.378	2.505	2.545	6.6	1.6
25	2.327	2.458	2.538	8.3	3.2
26	2.370	2.471	2.539	6.7	2.7
27	2.378	2.499	2.538	6.3	1.5
Avg.	2.338	2.486	2.539	7.9	2.1
Stdev.	0.047	0.015	0.003	1.85	0.57

Table 11. *Bulk specific gravies of cores for location C in the centerline of the road.*

Location C (centerline)					
Id	G_{mb} (DIM)	G_{mb} (SSD)	G_{mm}	V_a % (DIM)	V_a % (SSD)
1	2.387	2.482	2.542	6.1	2.3
2	2.398	2.499	2.539	5.5	1.6
3	2.356	2.500	2.541	7.3	1.6
4	2.296	2.486	2.533	9.3	1.8
5	2.338	2.490	2.534	7.7	1.7
6	2.379	2.482	2.532	6.0	2.0
7	2.348	2.487	2.535	7.4	1.9
8	2.426	2.495	2.543	4.6	1.9
9	2.227	2.484	2.538	12.3	2.1
Avg.	2.351	2.489	2.537	7.4	1.9
Stdev.	0.060	0.007	0.004	2.30	0.23

Table 12. *Bulk specific gravies of cores for location D in the right wheel path.*

Location D (right wheel path)					
Id	G_{mb} (DIM)	G_{mb} (SSD)	G_{mm}	V_a % (DIM)	V_a % (SSD)
10	2.265	2.471	2.541	10.9	2.8
11	2.246	2.467	2.541	11.6	2.9
12	2.212	2.462	2.542	13.0	3.2
13	2.317	2.488	2.530	8.4	1.7
14	2.332	2.451	2.537	8.1	3.4
15	2.343	2.477	2.546	8.0	2.7
16	2.378	2.485	2.545	6.6	2.3
17	2.384	2.473	2.538	6.1	2.6
18	2.322	2.471	2.543	8.7	2.8
Avg.	2.311	2.472	2.540	9.0	2.7
Stdev.	0.059	0.011	0.005	2.32	0.49

6.2.3 *VNA measurements*

The VNA measurements were conducted using the transmission method of measuring through the sample (see Figure 38). Measurements were taken using two volume elements with a frequency sweep of 7 to 17 GHz. First, a point measurement with the effective antenna footprint of ca. 20 x 20 mm^2 on the sample surface was used. Then, two samples were 2D scanned with scanning area of 75 x 75 mm^2. Results are given in Table 13 below.

Figure 38. a) *VNA apparatus, (b) core sample measurement set up on the right.*

From the measured amplitude (A) and phase (φ), the dielectric constant ε_r' was then obtained by modified linear regression. However, the VNA recordings required some post-processing before we received the desired dielectric parameters of the sample under test. This is illustrated in Figure 38 below. The raw VNA data contains the signal attenuation of the sample, expressed in dB, and the relative phase angle in degrees. Initially, the phase data must be unwrapped, which means adding a required amount of 360-degrees steps to it to avoid ambiguity. However, multiple reflections on the sample-air interfaces, both in front of it and at the back, cause the phase plot to wobble somewhat; therefore, simple linear regression calculus would not alone produce a correct group delay of the sample. Instead, we spotted those points of the phase curve, which matched either local amplitude maxima or minima in the attenuation plot. These points have been marked in Figure 38 with vertical lines. The regression algorithm was then applied only to those phase values and a correct group delay obtained. From it, we defined the real part of permittivity in a normal way.

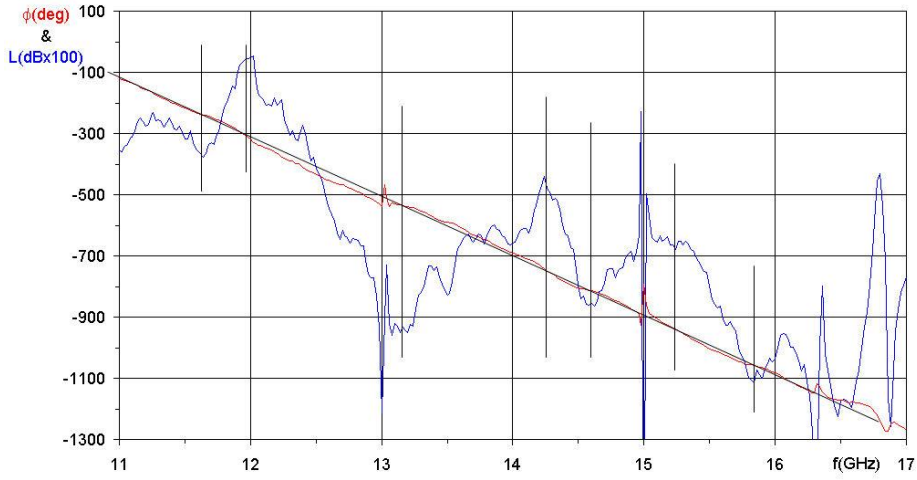

Figure 39. *Modified linear regression is applied to the VNA-based phase plot. Only those phase values which match local amplitude maxima or minima are used.*

Eq. (23) is then used to obtain dielectric constant ε_r' by knowing the thickness h of the specimen. Derivation of Eq. (23) is presented below (all parameter are defined in the Glossary of Symbols). The phase φ is in degrees, thus, it must be converted to radians by dividing it by 360 degrees and multiplying by 2π.

$$\lambda = v/f \ = c_0/(\sqrt{\varepsilon_r'}\, f) \tag{18}$$

$$(h/\lambda_a - h/\lambda_b) = \Delta\varphi\ 2\pi/360^\circ \tag{19}$$

$$h\left(f\sqrt{\varepsilon_{ra}'}\,/c_0 - f\sqrt{\varepsilon_{rb}'}\,/c_0\right) = \Delta\varphi\ 2\pi/360^\circ \tag{20}$$

Recognizing that the measurement is done in air, then the ε_{rb}' has a value of 1.

$$fh/c_0\left(\sqrt{\varepsilon_{ra}'} - 1\right) = \Delta\varphi\ 2\pi/360^\circ \tag{21}$$

The label from ε_{ra}' can be dropped and then solved for ε_r'

$$\varepsilon_r' = (2\pi\Delta\varphi c_0/(360^\circ hf) + 1)^2 \tag{22}$$

and finally the dielectric constant value ε_r' is:

$$\varepsilon_r' = (2\pi\Delta\varphi\lambda_{air}/(360^\circ h) + 1)^2 \tag{23}$$

The microwave frequencies used have a wavelength less than 40 mm allowing us to see more closely the granularity of asphalt compared with the bulk properties of asphalt measured by the GPR. However, as the VNA point measurement is only ca. 2% from the core volume, it may be too small relative to the measured bulk density of the core. Figure 40 shows a picture of core no. 11 and the scanning area 75 x 75 mm^2 superimposed over the core's surface area. Now the MVE is ca. 32% of the core volume and the scanned results should have a better match for the bulk density of the cores. Based on test results, shown in Table 13, this is indeed the case as both scanned VNA measurements give lower permittivity values than the point measurement, which we considered a better match to the conventional measurement of core density.

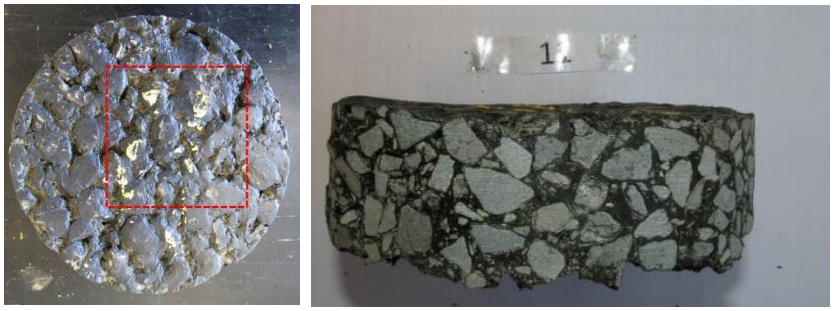

Figure 40. *Core sample no. 11: scanned area on the left and side view of the core on the right.*

Table 13. *VNA results for all cores. Measurements were taken using 7 to 17 GHz frequencies.*

C (centerline)			D (right wheel path)				A (centerline)		
Id	Thick. (mm)	Point ε_r'	Id	Thick. (mm)	Point ε_r'	Scanned average ε_r'	Id	Thick. (mm)	Point ε_r'
1	43	5.85	10	47	5.78	-	19	-	-
2	45	5.90	11	44	5.78	5.41	20	46	5.51
3	49	6.11	12	42	6.08	-	21	48	5.49
4	43	6.86	13	46	5.47	-	22	45	6.13
5	43	7.64	14	42	5.74	5.67	23	43	5.95
6	48	5.65	15	41	5.48	-	24	44	5.84
7	42	5.88	16	48	5.92	-	25	44	5.83
8	43	5.26	17	53	5.33	-	26	43	5.80
9	48	5.72	18	41	6.04	-	27	42	5.19
Avg.		6.10	Avg.		5.74	-	Avg.	46	5.72
Stdev.		0.72	Stdev.		0.26	-	Stdev.		0.30

6.2.4 *Comparison of MVEs*

Table 14 and Figure 41 compare MVEs for the electromagnetic and traditional measurements using the bulk properties by averaging core measurements at each location A, C and D. The overall bias in the measurements depends on the method of obtaining core density. The core dimensions revealed average air voids of 8.1% and the SSD method 2.2%. Interestingly, as the MVE increases, the ε_r' value decreases. This suggests that the electromagnetic methods "see" more aggregates when the volume element decreases. This seems a logical result as the highest permittivity values were obtained for the VNA point measurements with the smallest MVE at microwave frequencies.

Table 14. *Summary of results for all MVEs.*

Locations	1. GPR cont. ε_r'	2. GPR stat. ε_r'	5. VNA scan ε_r'	6. VNA point ε_r'	3. Cores V_a % (DIM)	3. Cores V_a% (SSD)
A	5.0	5.4	-	5.7	7.9	2.1
B	5.3	5.4	-	-	-	-
C	5.1	5.7	-	6.1	7.4	1.9
D	5.4	5.4	5.5	5.7	9.0	2.7
ALL Avg.	5.3	5.5	5.5	5.9	8.1	2.2

Figure 41 shows that, overall, the VNA point measurements did not capture the bulk properties of cores. This is confirmed by Figure 42, which reveals that there was no correlation between the air voids obtained from 150-mm diameter cores and the VNA point measurements. Nevertheless, the results are quite comparable with the prediction of the linear mixing model.

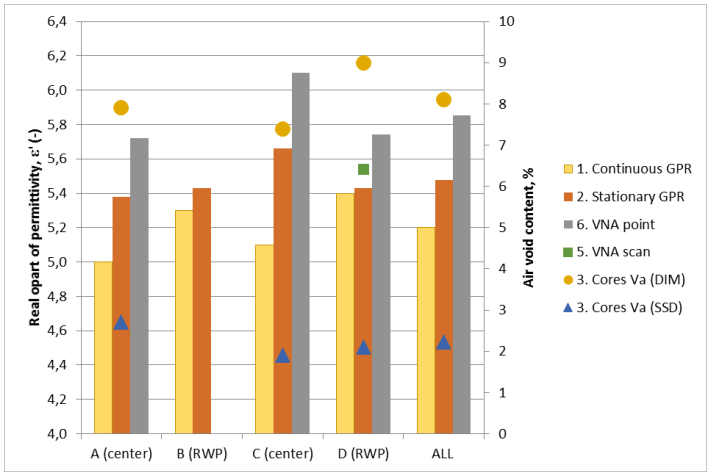

Figure 41. *Comparison of material properties with variable MVEs. Air voids of cores are presented in the y-axes on the right and dielectric properties are on the y-axes on the left.*

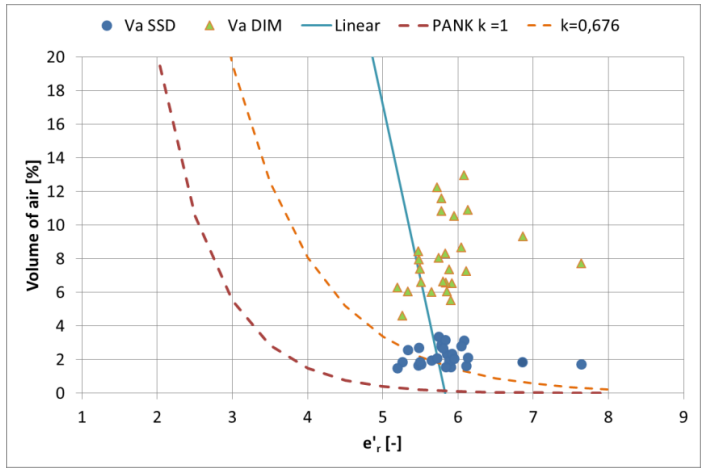

Figure 42. *Correlation of air voids with MVE-4 and VNA point measurements with MVE-6.*

6.2.5 *Conclusions*

There are a number of methods available to obtain asphalt density, each one using a slightly different method of determining the specimen volume. This will result in a varied precision when determining the air voids of the mixture. However, all the mixtures are measured with a similar precision using nondestructive electromagnetic methods. There are two measuring methods that were applied to asphalt: a free space transmission method in the laboratory, in which the material under test has been placed between two antennas; and the reflection measurement method or the radar principle, in which the reflected waves from the surface are used. The precision of these two methods for measuring asphalt is not known at the moment.

On average, the test results of this study agreed with theoretical formulations with the air voids increasing as the dielectric property ε_r' decreased. Significantly, when the measured volume element (MVE) increased the ε_r' value decreased. This suggests that the electromagnetic methods "see" more aggregates when the volume element decreases. Therefore, it can be concluded that the RVE for the EM-measurements is highly frequency dependent.

The VNA measurements were conducted with an RVE of ca. 2% and 32% of drill core volume. The smaller one was revealed to possess an insufficiently small volume element resulting it in being unreliable for reference measurements of the individual cores. More studies are needed for the recommendations of acceptable RVE; however, a larger area than the RVE of 2% must be measured if one wants to correlate dielectric properties with the bulk properties of asphalt.

The results showed that the GPR measurement method with a footprint of 0.3 x 1 m averaged the air voids variation ranging from 1.5 to 3.4% for the SSD method and 4.6 to 13% for the DIM method for pavement overlaid with SMA16 mixture. Therefore, using only one core for calibrating the GPR is not recommended because the MVE is too small relative to the required RVE. A further issue is the influence of lower layers on the GPR-based ε_r' values, particularly when the asphalt to be measured is only 40 mm thick.

6.3 Results for raw materials

6.3.1 *Aggregate permittivity*

A visual inspection revealed that there were two different rock types in the SMA aggregate blend. The majority of the aggregate ca. 80 % was dark metavolcanic rock with intermediate composition and the rest was pegmatite. The permittivity of aggregates collected from the quarry were measured in this study applying three different methods.

Figure 43 shows the cavity resonator measurement arrangement (6-8 GHz) and the cut-off method with the circular waveguide antenna with the stone filling method. For the methods, polished aggregate buttons had to be manufactured as is shown in Figure 44. The third method used was the VNA free-space transmission configuration with a frequency of 7 to 17 GHz. The measured specimen was a rock slab with the dimensions of 205 x 245 mm and the measurement footprint was approximately a circle with ca. 20 mm diameter. The dielectric constant ε_r' values differed clearly for two different rock types.

The average permittivity values from all three methods were 4.7 for the pegmatite and 6.20 for the metavolcanic rock. A larger variation for the VMA measurements shows that there was some material variation in the rock slab. A more detailed analysis of these results can be found in Olkkonen et al. (2014).

Table 15. *Summary of and rock aggregate dielectric constant ε_r' results.*

Rock type	Method	n	Avg.	St.dev.	Source of variation
Pegmatite	Cavity resonator	21	4.55	0.04	Some material + test method
	Cut-off	1	4.76	-	
Intermediate metavolcanic rock	Cavity resonator	21	6.24	0.07	Some material + test method
	Cut-off	1	6.17	-	
	VNA (rock slab)	9	6.20	0.22	Material + test method

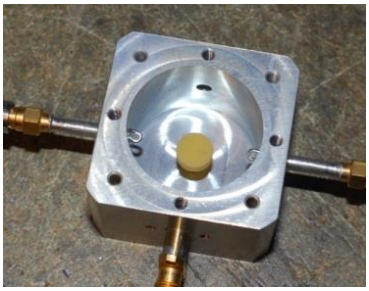
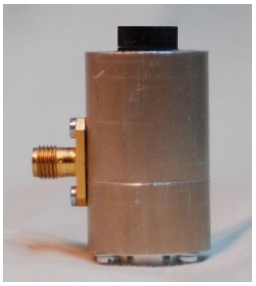

(a) (b)

Figure 43. *Measurement methods: a) Cavity resonators; b) circular waveguide cut-off*


(a) (b)

Figure 44. S*pecimen preparation for permittivity measurements (a) sampled aggregate, (b) fabricated rock buttons.*

6.3.2 *Bitumen permittivity*

There is five to six percent bitumen in the asphalt mixture. It became evident that the dielectric values reported in the literature were not based on actual measurements as the same values seemed to be cross-referenced amongst researchers. Therefore, we decided to measure the permittivity.

This was not an easy task and after several trials and errors, four reasonably good bitumen slabs were finally prepared. It was important to extract all the air when pouring bitumen into the mold as brittle specimens broke easily (see Figure 45). Two bitumen grades were tested 70/100 and a softer grade of 160/220. Specimens were kept in a freezer before the measurements to prevent slabs from deforming and crumbling. However, during measurements they started to warm up, soften very quickly and collect moisture from the air, which caused errors as results indicate.

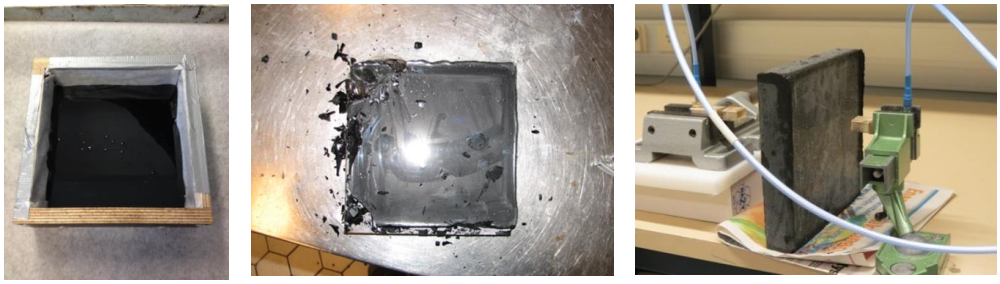

(a) (b) (c)

Figure 45. *Preparing bitumen slabs for measurements and measurement arrangement.*

Table 16 reveals the results. At 7 to 17 GHz, bitumen ε_r' was measured to be 2.54 (0.32) for 70/100 specimens. For 160/220 variation was larger and average was higher being 3.25 (1.48). Results for the bitumen 70/100 accord with values from the literature; however, softer bitumen results are obviously too high due to problems in testing.

Table 16. *Permittivity measurement results for bitumen slabs.*

Bitumen grade	Thickness	ε_r' 7-17 GHz						ε_r' 5-7 GHz
	(mm)	A	B	C	D	Avg.	St.dev.	
Slab 70/100	10	2.3	2.4	3.1	2.5	2.6	0.36	-
Slab 160/220	10	4.3	-	-	-			-
Slab 70/100	40	2.4	3.1	2.5	2.4	2.6	0.34	-
Slab 160/220	40	2.2	-	-	-			3.4-3.8

6.4 Vt12 pavement slabs and cores

6.4.1 *Pavement slabs: Density and permittivity results*

As discussed in Chapter 4, we managed to extract only two slabs from Vt12 because the other two slabs were damaged during sampling. From Vt3, we did not manage to recover any slabs. The slabs were first measured using a 1.2-2.2 GHz antenna transmission arrangement as shown in Figure 46 below. The footprint of the measurements was ca. 100 x 200 mm, in other words, the area size of the antenna. Then, the point measurements were taken with 7 to 17 GHz transmission measurement arrangement. Measurements were centered from the middle of the slab and then shifted horizontally and vertically at an interval ca. 6 and 12 mm. Pont G, where Slab 4 had the highest thickness, was measured three times. The results are in Table 17. Slab 1 was too thin to be measured reliably as its thickness ranged only from 23-28 mm, whereas Slab 4 was ca. 32 mm thick. However, even that thickness may have been too thin for reliable measurements. For Slab 1, the average ε_r' was 5.03 and for the Slab 4 it was 4.61 – 4.8. As Figure 35 indicates, the condition of Slab 1 was visually worse than that of Slab 4 although the variability of measurements is comparable. Pavement density was measured using the air-water volume method and both slabs had very similar air voids of 7.2 (Slab 1) and 7.3 (Slab 4) percent.

Table 17. *Vt12 slabs VNA measurements for* ε_r'.

Location	1.2-2.2 GHz	1.2-2.2 GHz	7-17 GHz
	Slab 1	Slab 4	Slab 4
Point A	4.9	4.8	3.9
Point B	5.6	4.2 – 6.5	4.2
Point C	5.1	-	5.7
Point D	5.1	-	7.0
Point E	-	-	4.0
Point F	-	-	4.8
Point G1 (38 mm)	-	-	4.2
Point G2 (38 mm)	-	-	3.9
Point G3 (38 mm)	-	-	3.8
Average	**5.03**	**ca. 4.8**	**4.61**
St. dev.	**0.93**	**-**	**1.08**

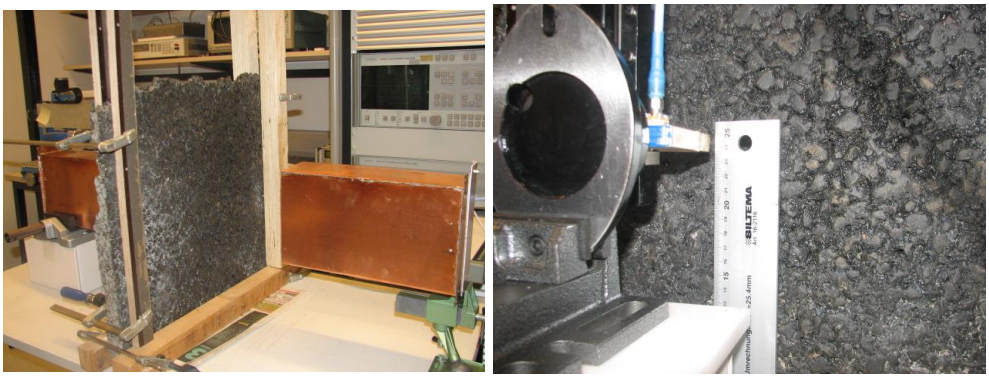

Figure 46. *VNA transmission measurements arrangement for the large slab; left 1.2-2.2 GHz and right 7 -17 GHz.*

6.4.2 *Pavement cores: Density and permittivity results*

For Vt12, we took ten cores, but they were only 100 mm in diameter; therefore, the core diameter was too small for reliable VNA measurements. The permittivity of the cores was measured using a transmission method with 7 to 17 GHz frequency applying the point method - only one reading was obtained. The results are given in Table 18 with laboratory density measurements.

Table 18. *Vt12 density measurements for 100-mm cores and point VNA measurements for* ε_r'.

Id	Thick. (mm)	G_{mb}			G_{mm}	Va (%)			VNA-1 ε_r'	VNA-2 ε_r'
		SSD	DIM	Paraf.		SSD	DIM	Paraf.		
S1	74	2.430	2.301		2.537	4.2	5.9	-	7.54	5.80
S2	42	2.409	2.162	2.326	2.515	4.2	11.3	7.7	5.41	7.91
S3	40	2.435	2.263	2.304	2.513	3.1	7.1	8.6	7.68	4.93
S4	39	2.438	2.231	2.290	2.507	2.8	9.7	9.2	8.7	9.59
S5	39	2.427	2.263	2.246	2.524	3.8	9.7	10.9	7.92	8.54
S6	39	2.424	2.164	2.243	2.530	4.2	11.5	11.0	5.98	4.71
S7	42	2.411	2.201	2.217	2.538	5.0	14.3	12.0	6.63	5.38
S8	41	2.417	2.243	2.240	2.513	3.8	11.6	11.1	6.57	4.74
S9	44	2.392	1.736	2.158	2.513	4.8	18.0	14.4	4.89	4.64
S10	42	2.392	2.106	2.183	2.536	5.7	14.3	13.4	8.1	5.06
Avg.	41	2.418	2.167	2.245	2.523	4.2	14.1	10.9	6.94	6.13
St.dev.	1.71	0.016	0.162	0.055	0.012	0.861	6.39	2.18	1.25	1.84

Figure 47 shows that there is a faint correlation between ε_r' and air void content with low air voids translating to very high dielectric values. This confirms that in the VNA measurements the 100 mm core is too small to be used as the reference core. Figure 48 compares air void measurements conducted with three methods of SSD, DIM and Parafilm. It is obvious that the SSD method evens out the air voids variation in the core samples. The SMA16 mixture had large surface irregularities, which were not captured by measuring core dimensions as the regression lines in Figure 48 indicate.

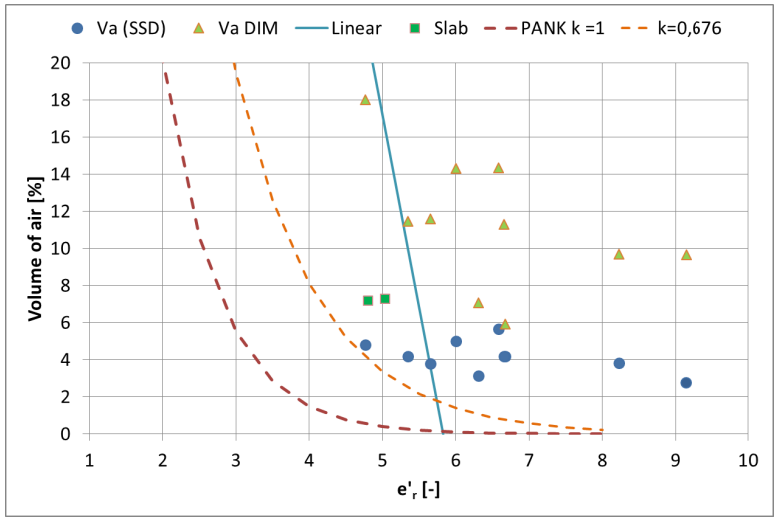

Figure 47. *Correlation of 100-cores between VNA measured* ε_r' *and air voids measured with SSD and DIM method.*

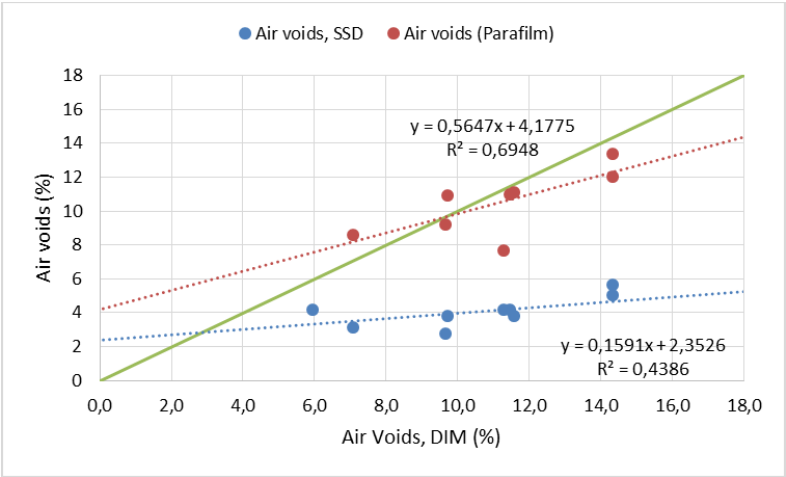

Figure 48. *Correlation of 100-mm cores air voids between DIM, SSD and Parafilm methods.*

6.5 Repeatability of measurements with VNA

6.5.1 *Point measurement repeatability for 150-mm cores*

The repeatability of point measurements was studied using 150 mm cores from Vt3. Three cores were selected based on their visual appearance. Judged visually, L2 was a good sample, L11 was an average sample, and L14 was a poor sample. The sample was placed into the sample holder and then taken out ten times repeating the measurement. The measuring distance was kept at 150 mm with the top of the core facing the sending antenna but the rotational orientation of the cores was not kept constant. These results are shown in Table 19.

Table 19. *Repeatability of point measurements for dielectric constant,* ε_r' .

	Thickness (mm)	n	Avg.	St.dev.	Var.	max-min	L(dB)
L2	45.0	10	5.19	0.108	0.012	0.26	3-5
L11	45.0	10	5.00	0.039	0.001	0.08	3-5
L14	41.0	10	6.21	0.964	0.930	2.61	7-15
L2	45.6	10	5.13	0.104	0.011	0.25	-
L11	44.5	10	5.06	0.043	0.002	0.09	-
L14	41.8	10	6.07	0.937	0.878	2.54	-

Results show that the point measurements produced varied results and variation can be up to one unit of ε_r' values. This confirms the results in the RVE experiments as well as the understanding that a larger spatial area than what the point measurement is capable of must be measured from the core. For sample L14, the loss of the signal is substantially larger indicating either the presence of large aggregate or some other lossy material buried inside the sample.

One important source of error is the thickness of the specimens. A 1 mm difference in a 50 mm thick specimen causes a 0.1 unit difference in the dielectric constant. If the electromagnetic

measurement method is capable of determining the thickness while measuring, this will not be a problem.

6.5.2 *Effect of slab thickness and its gradation variation*

A 25 mm x 75 mm (height x width) piece of Slab 1, which broke off from the larger piece, was measured with the asphalt scanner with 5 mm intervals to investigate the variation of measurements relative to thickness variations in the slab. The back side of the slab was quite uneven due to the sampling method (see Section 4.2) and the thickness varied ca. 25%, ranging from 28 to 39 mm (see Figure 49).

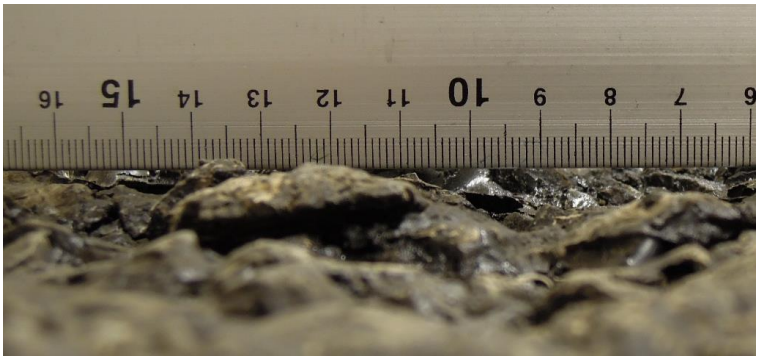

Figure 49. *Thickness variation of asphalt slab at the bottom.*

Figure 50 and Table 20 present the results of Slab 1. Calculations were carried out using a linear interpolation of the slab thickness which was based on measurements at certain locations. The average of all 70 measurements was 6.55 and the standard deviation of 1.08 indicated a very large variation. The minimum ε_r' value was 4.3 and maximum was 9.51. The difference was 5.21 units. This is much larger than the rock aggregate dielectric variation of 0.22 measured from the rock slab. Therefore, most of the variation can be attributed to the air, gradation and binder content variation. The repeatability measurement of core L14 gave a variation of 0.94 which is comparable to the slab measurements.

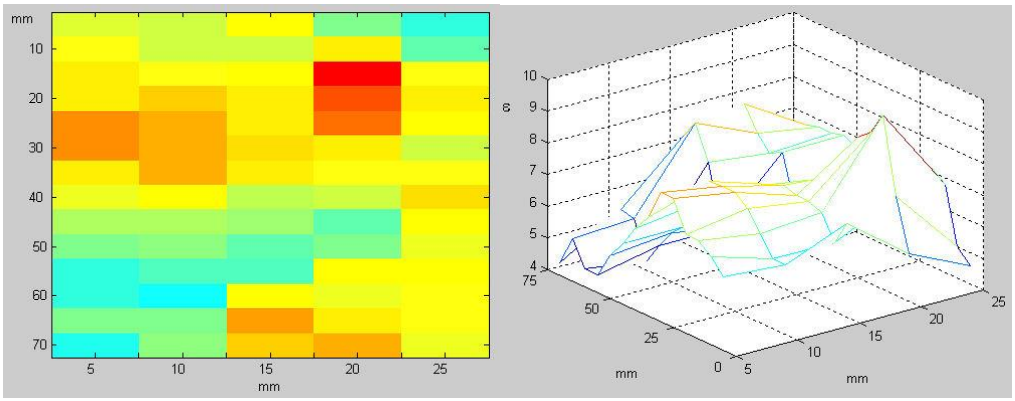

Figure 50. *Variation of VNA measured ε_r' values on asphalt slab measured at 5 mm intervals.*

Table 20. *Vt12 VNA scanner measurements of ε_r' for Slab 1.*

X/Y mm	5	10	15	20	25	Avg	St.Sev.
5	6.34	6.19	6.95	5.49	4.59	5.91	0.90
10	6.8	6.19	6.19	7.11	5	6.26	0.81
15	7.11	6.8	6.95	9.51	6.8	7.43	1.17
20	7.11	7.43	7.11	8.79	7.11	7.51	0.73
25	8.1	7.76	7.11	8.44	6.95	7.67	0.64
30	8.1	7.76	7.27	7.11	6.22	7.29	0.72
35	7.11	7.72	7.11	6.82	6.83	7.12	0.37
40	6.57	6.84	6.04	6.17	7.25	6.57	0.49
45	5.93	5.93	5.71	5.06	6.99	5.92	0.69
50	5.36	5.57	5.16	5.36	6.65	5.62	0.59
55	4.58	4.96	4.96	6.88	6.88	5.65	1.13
60	4.58	4.3	6.88	6.65	6.76	5.83	1.28
65	5.36	5.46	7.95	7.11	6.76	6.53	1.11
70	4.4	5.57	7.35	7.83	6.65	6.36	1.39
Avg.	6.25	6.32	6.62	7.02	6.53	**6.55**	
St.dev.	1.25	1.10	0.88	1.30	0.78		**1.08**

7 ANALYSIS OF GPR MEASUREMENTS

7.1 Descriptive statistics

Figure 51 and Figure 52 present dielectric constant values for continuous GPR measurements. At Vt3, the old pavement surface was more variable and the magnitude of ε_r' was more than two units higher than after resurfacing. Appendix A shows that the thickness of the old pavement was only 130 mm, which is in the borderline of 1 GHz GPR depth resolution. Also, moist unbound granular layers may have increased the magnitude of permittivity readings. Thickness increased to 170 mm after the SMA layer was added and the radar signal was now confined into the asphalt layers. This may explain the drop of permittivity values compared with the results obtained from the thinner pavement structure. Both measurement paths, the centerline and right wheel path, seem to follow similar trends although the right wheel path gave higher values, except for the last measurement taken 40 days after construction. Figure 50 shows that at Vt12 there is a sharp increase in permittivity values towards the end of the measurement section. Cores and stationary measurements were taken from this area of higher dielectric values. A reason for this increase is not apparent.

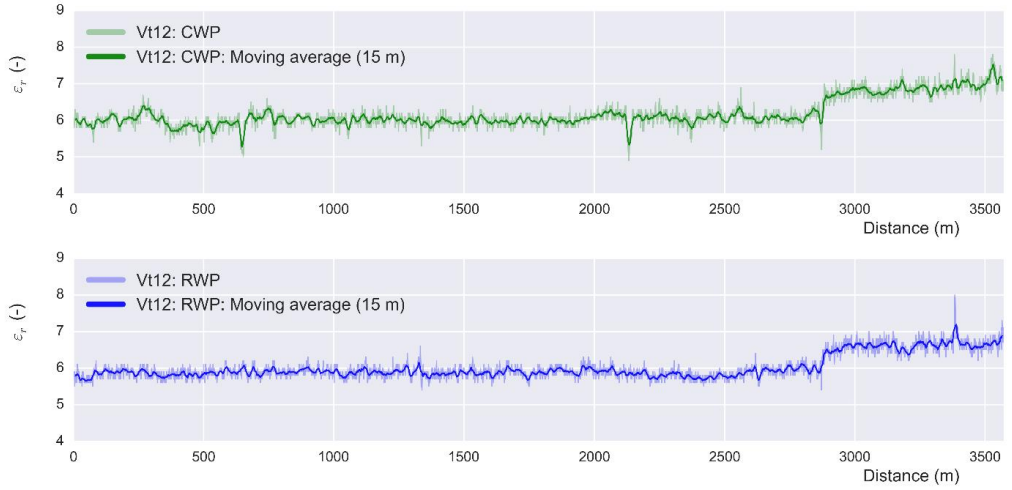

Figure 51. *GPR measurements for Vt12.*

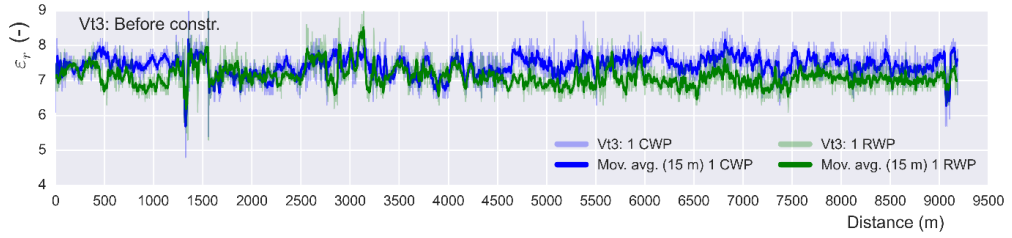

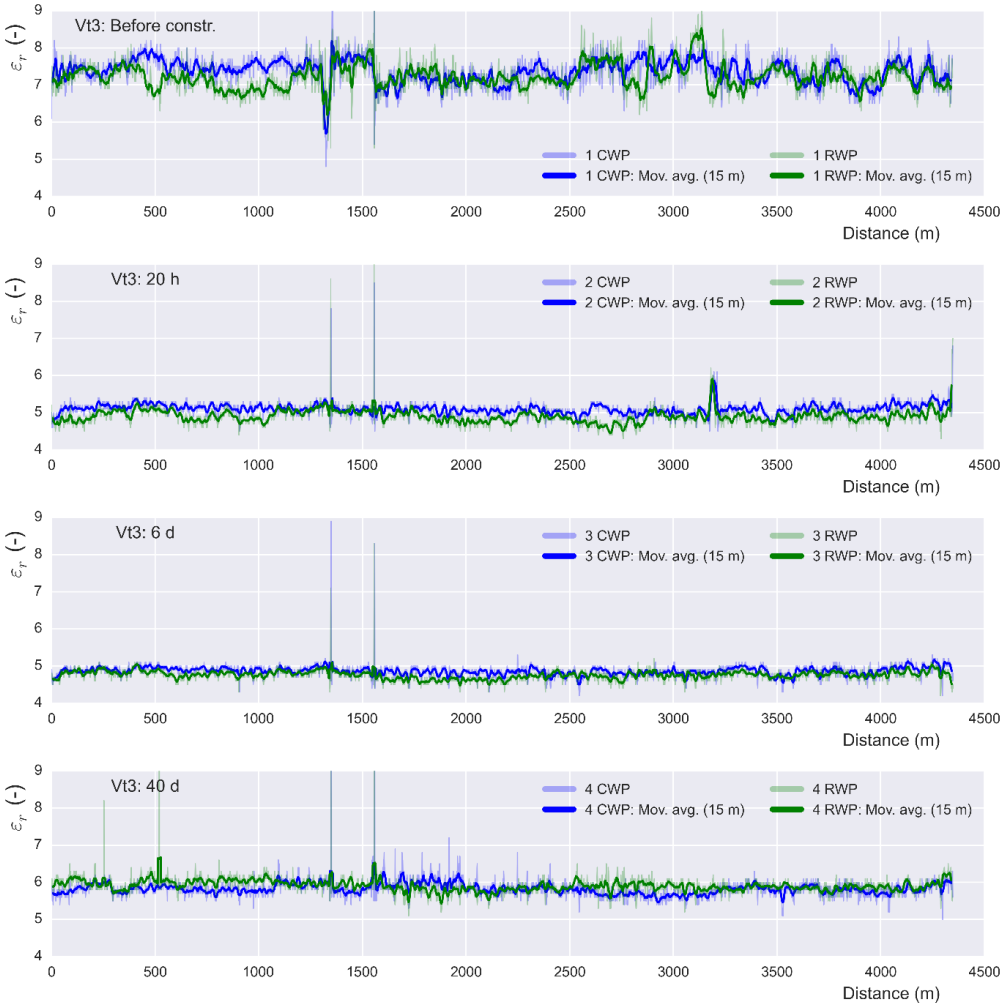

Figure 52. *GPR measurements for Vt3 (9500 m). Runs before construction have been presented in two ways: first, the whole test section, and then, only the stretch of road (4500 m) that was measured repeatedly.*

The summary values shown in Table 21 to Table 23 are calculated from data retrieved from the RoadDoctor software where data was processed after the measurements. Standard deviation represents the variation of each one-meter stretch of the road averaged by the post-processing software. Outliers, such as reflections from bridge structures, have been excluded. Table 21 and Table 22 show that at Vt12 the magnitude of ε_r' was higher and the variations were larger compared with Vt3. Even before construction, Vt3 had less variation in measured permittivity values, but magnitudes were similar. As the permittivity of water is 80, it is possible that moisture infiltration into the pavement structure has contributed to these results on Vt12 and Vt3 before construction. Therefore, it is conceivable that the measurement time, indeed, the date, as well as pavement thickness, are responsible for the actual magnitude of permittivity at any given time of measurements. Table 23 indicates results for stationary measurements. Total variation has been calculated to include material variation by averaging all locations A to D for

Vt3 and 1 to 7 for Vt12. Below these summary statistics, there are results for the pooled variances marked with an asterisk. This variation excludes the material variation and is indicative of the GPR testing variation. Notably, at Vt12, the stationary testing variation is twice the variation at Vt3.

Table 21. *Summary of continuous scan dielectric constant ε_r' values for Vt3.*

Time	Location	Mean	St.dev.	Min	Max	Count	CV%	Se
Before constr.	**center_1**	7.4	0.35	4.8	8.7	9185	4.7	0.0037
B. constr. Truncated	**center_1**	7.4	0.37	4.8	8.6	4346	5.0	0.0056
20 h	**center_2**	5.1	0.16	4.5	6.2	4346	3.1	0.0024
6 days	**center_3**	4.9	0.13	4.2	5.3	4349	2.7	0.0020
40 days	**center_4**	5.8	0.18	5	6.9	4346	3.1	0.0027
Before constr.	**rw_1**	7.1	0.34	5.3	8.9	9182	4.7	0.0035
B. constr. truncated	**rw_1**	7.2	0.37	5.3	8.9	4348	5.2	0.0057
20 h	**rw_2**	4.9	0.18	4.3	6.2	4342	3.6	0.0027
6 days	**rw_3**	4.8	0.13	4.2	6.3	4349	2.6	0.0019
40 days	**rw_4**	5.9	0.17	5.1	6.6	4343	2.9	0.0026

Table 22. *Summary of continuous scan dielectric constant ε_r' values for Vt12.*

Time	Location	Mean	St.dev.	Min	Max	Count	CV%	Se
76 days	**Center**	6.2	0.40	4.9	7.8	3573	6.4	0.0066
	Rw	6.0	0.33	5.4	8.0	3573	5.6	0.0056

Table 23. *Summary of stationary scan dielectric constant ε_r' values.*

Time	Location	Mean	St.dev.	Min	Max	Count	CV%	Se
76 days	**VT12_1**	6.9	0.14	6.4	7.4	1405	2.1	0.0039
	VT12_2	7.2	0.13	6.7	7.6	1360	1.8	0.0035
	VT12_3	7.5	0.14	7.1	7.9	1355	1.8	0.0037
	VT12_4	7.8	0.16	7.2	8.2	1295	2.1	0.0045
	VT12_5	7.1	0.12	6.6	7.4	1349	1.7	0.0032
	VT12_6	7.1	0.14	6.6	7.4	1385	1.9	0.0037
	VT12_7	7.2	014	6.7	7.6	1350	1.9	0.0038
20 h	**VT3_A**	5.4	0.04	5.3	5.4	99	0.7	0.0040
	VT3_B	5.4	0.06	5.3	5.6	99	1.2	0.0063
	VT3_C	5.7	0.05	5.5	5.7	99	1.0	0.0054
	VT3_D	5.4	0.06	5.3	5.6	99	1.2	0.0064
76 days	**VT12_total**	7.2	0.30	6.4	8.2	9499	4.2	0.0031
20 h	**VT3_total**	5.5	0.12	5.3	5.7	396	2.7	0.0060
76 days	**VT12_total**	7.2	0.14*	6.9	7.8	7	1.9	0.0529
20 h	**VT3_total**	5.5	0.06*	5.4	5.7	4	2.0	0.03

Figure 53 and Figure 54 provide the histograms of measurements in the form of Kernel density estimates. Figure 53 confirms that variation of dielectric values at Vt3 increases during the in-service period of the road. Figure 54 shows that at Vt12 there are two different peaks in the density function. This confirms that there are two different blocks of data on the dataset.

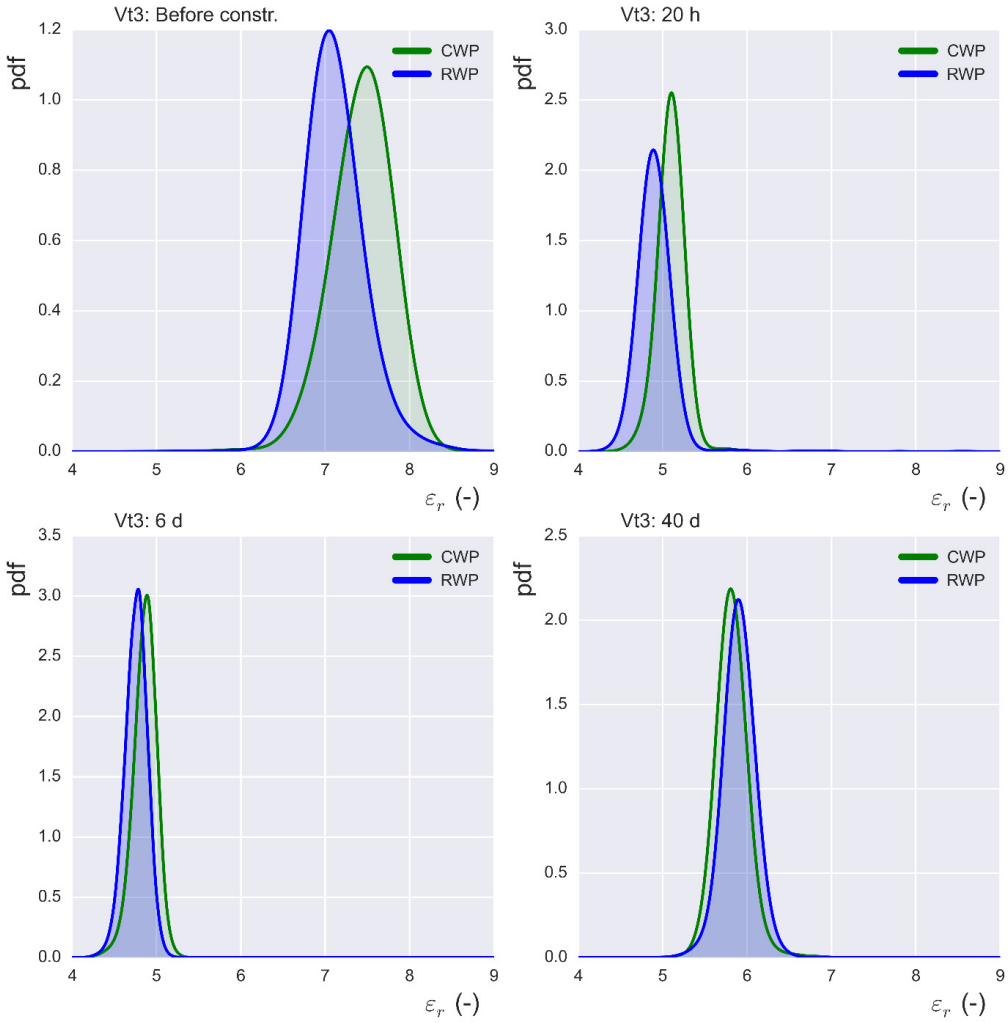

Figure 53. *Histograms of Vt3 measurements for* ε_r'.

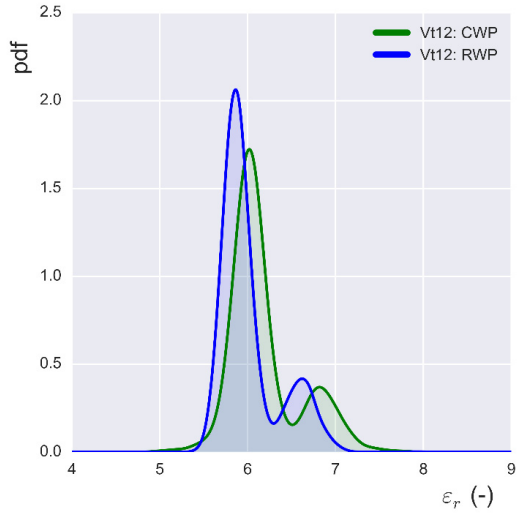

Figure 54. *Histograms of Vt12 measurements for* ε_r'.

7.2 PANK Calibration method

7.2.1 *Influence of a single core*

The PANK calibration factor *k* was calculated by applying the marker-method with stationary measurements as is explained in Section 4.2. In addition, the continuous GPR measurement dataset was analyzed to match the permittivity measurements at the core location for computing the *k* value.

Calibration was first conducted using all 26 cores from Vt3 using continuous measurements matched to the core locations. Location A included cores from 20 to 27, location C had cores from 1 to 9 and location D had cores from 10 to 18. The ε_r' values were 5.0 5.1 and 5.4 for locations A, C and D, respectively. The average ε_r' of these 4 readings was 5.2 and the standard deviation was 0.16. The average air void content for these four locations of ca. 20 m^2 was 2.2 % (n=27) with a standard deviation of 0.56.

Figure 55 shows the dramatic influence a single core location has on the average air voids; within a small area of 0.5 m x 0.5 m, there could be up to 1.7 % difference between cores as location D reveals, and any of the cores may end up as a calibration core.

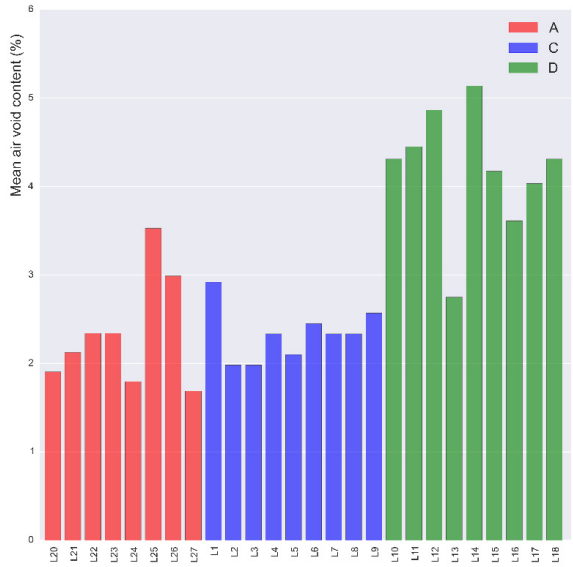

Air voids SSD (%)

Location A

3,2	2,7	1,5
2,1	2,1	1,6
	1,7	1,9
Avg	2,1	
Std.	0,6	

	ε_r
A	5,0
C	5,1
D	5,4

Location C

1,9	1,9	2,1
1,9	1,7	2
2,4	1,6	1,6
Avg	1,9	
Std.	0,3	

Location D

2,3	2,6	2,8
1,7	3,4	2,7
2,8	2,9	3,2
Avg	2,7	
Std.	0,5	

Figure 55. *Influence of a single core on the average air voids of measured road Vt3.*

7.2.2 *Influence of measuring path and measuring date*

To better understand the possible variations associated with the PANK calibration process, both measurement locations, the right wheel path (RWP) and the center wheel path (CWP), were employed in the process. In addition, data sets measured at different dates were used. Figure 56 show that the measurement location has a profound influence on the obtained results. The right wheel path provided higher air void contents and variation was larger than in the CWP. This may indicate problems in rolling, as the deep rut depth may prevent proper rolling of mixture placed on the rut. For Vt3, the old surface was milled and then filled with mixture; therefore, one could assume that the surface base layer was evenly stiff and there should not be any reflections of rutted areas.

Figure 57 shows the evolution of RWP rutting as time passes from construction. Porous SMA pavements will collect water during rain. This will increase dielectric values above the ε_r' value equivalent to the maximum density of a dry asphalt mixture as discussed before. On the other hand, there may be densification in the rut, which in turn will increase dielectric constant values.

To see if the same phenomenon is present in the center of the road, Figure 58 shows the evolution of air void content for CWP.

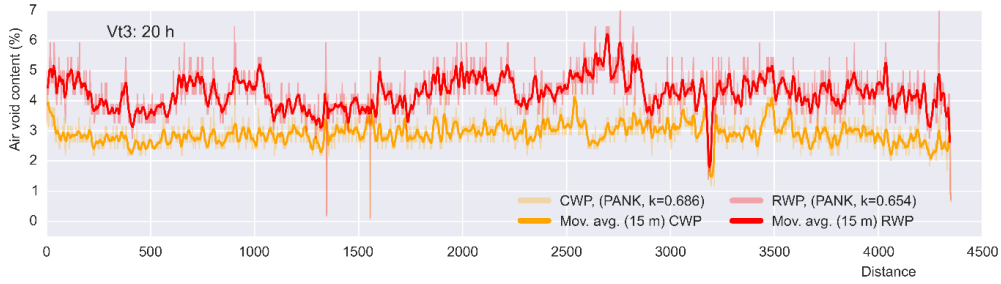

			Calib. core	ε_r'	k	Avg.	St.dev.	n
Stationary	20 h	RWP	2.7 %	5.6	0.686	4.3 %	0.65 %	4350
Stationary	20 h	CWP	2.0 %	5.4	0.654	2.9 %	0.42 %	4349

Figure 56. *Calibrated air void content for Vt3 for 20 h GPR measurements.*

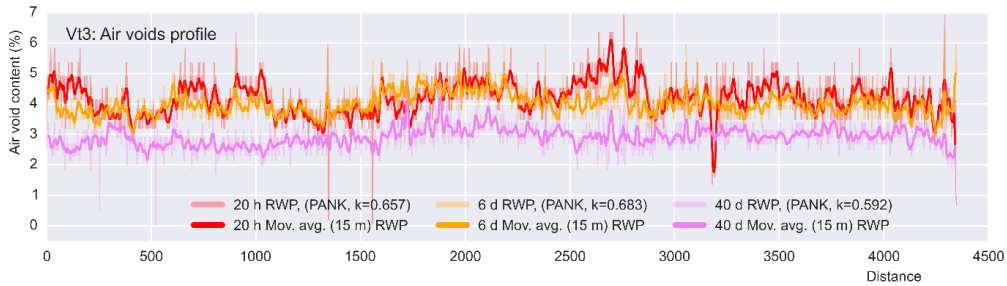

			Calib. core	ε_r'	k	Avg.	St.dev.	n
Continuous	20 h	RWP	2.7 %	5.4	0.657	4.2 %	0.64	4350
Continuous	6 d	RWP	2.7 %	5.2	0.683	4.0 %	0.46	4351
Continuous	40 d	RWP	2.7 %	6.0	0.592	2.9 %	0.40	4348

Figure 57. *Evolution of RWP rut depth porosity for Vt3.*

			Calib. core	ε_r'	k	Avg.	St.dev.	n
Continuous	20 h	CWP	2.0 %	5.1	0.749	1.9	0.3	4349
Continuous	6 d	CWP	2.0 %	5.0	0.765	2.2	0.3	4351
Continuous	40 d	CWP	2.0 %	6.0	0.636	2.2	0.33	4349

Figure 58. *Evolution of CWP rut depth porosity for Vt3.*

Figure 59. *Histograms of calibrated air void content variation for Vt3.* shows histograms of calibrated air void content values shown in the figures above. RWP has more variation at the beginning and variation seems to decrease with time. It is not quite clear if this is a true phenomenon or an artifact of the calibration process.

Figure 60 gives the results for the Vt12 measurements. There were 76 days between construction and GPR runs, and the data set was not uniform. The stationary measurements had quite a high standard deviation compared with the Vt3 results, which suggest some problems in the actual measurements as material variation should not be present. As Figure 60 shows, using stationary measurements as a reference will result in air void content values of

around ten percent. When continuous results are used, air void content level drops to ca. five percent. The last 500 meters seems to have a very different level of air voids, which seems to be quite unrealistic. Figure 61 depicts histograms of calibrated values.

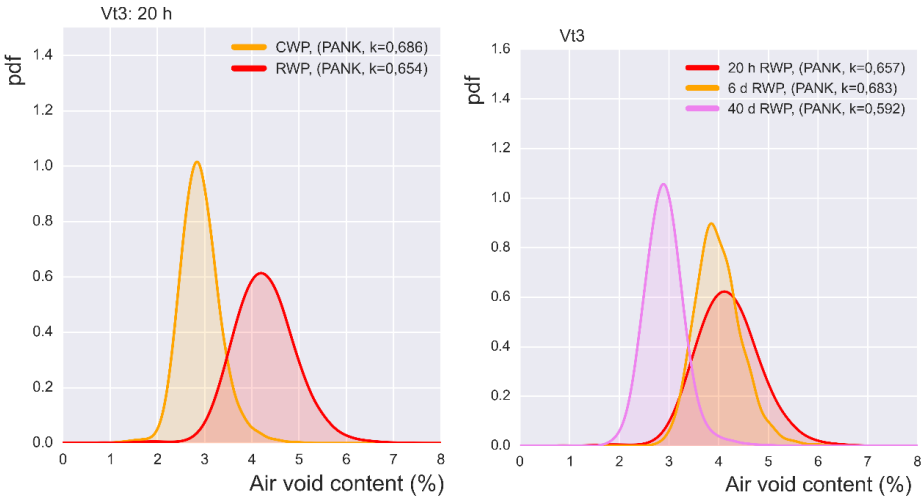

Figure 59. *Histograms of calibrated air void content variation for Vt3.*

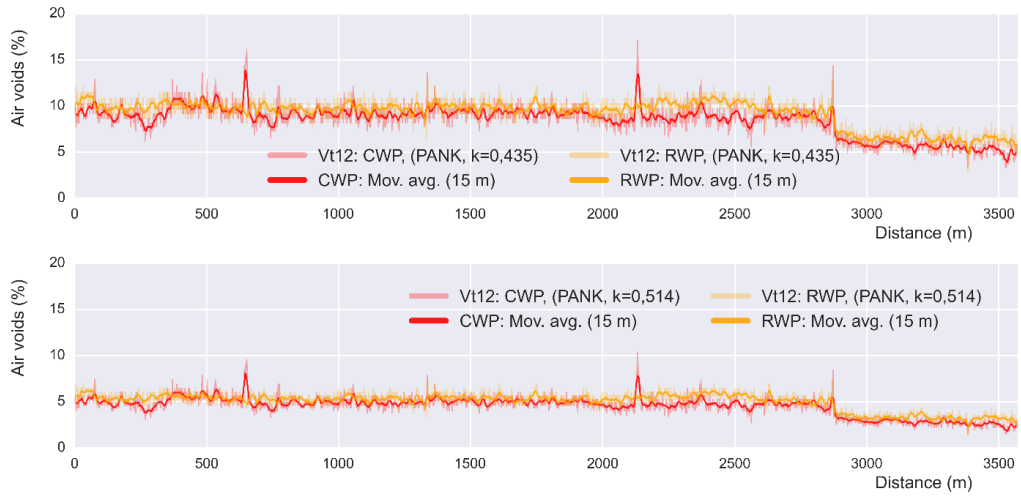

			Calib. Core	ε_r'	k	Avg.	St.dev.	n
Stationary	76 d	RWP	4,6 %	7,2	0,435	9,2	1,55	3572
Stationary	76 d	CWP	4,6 %	7,2	0,435	8,5	1,71	3572
Continuous	40 d	RWP	4,2 %	6,1	0,514	5,0	0,97	3572
Continuous	40 d	CWP	2,7 %	6,0	0,514	4,5	1,06	3572

Figure 60. *Calibrated air void content for Vt12.*

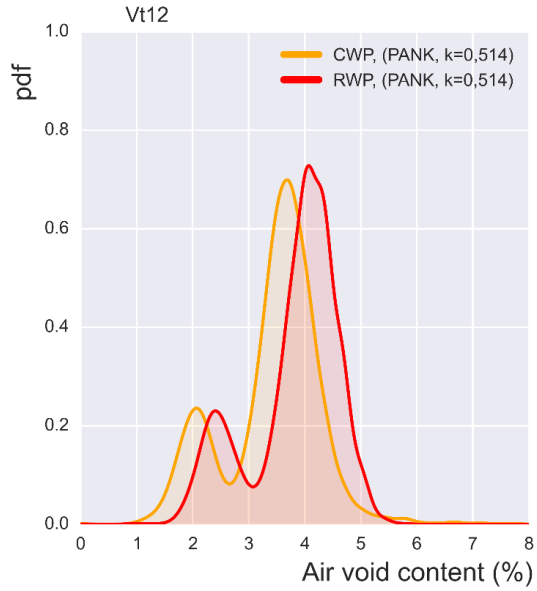

Figure 61. *Histograms of calibrated air void content variation for Vt12.*

Table 24 shows the Finnish Transport Agency's QA measurements after construction. The measurements were conducted with a GPR of GSSI/Sir -20 with a 1.0 GHz antenna. The report stated that there were no values below the lower limit of 1 percent of air. There were 12 m and 1 meter of road for Vt12 and Vt3, respectively, above the higher air voids level of 6 %. Calibration was conducted using the marker-method. Overall, air voids variation of 0.32-0.34 is unrealistically low as has been earlier discussed. The average air void contents of 2.9 % for Vt3 is comparable to our results, but for Vt2 measurements suggest a lower average air void content.

Table 24. *Summary of QC stationary scans dielectric constant ε_r' values.*

Road	Date	Length (m)	Road registry	GPR ε_r' (-)	Single core V_a (%)	Calibrated air voids, (%)	
						Avg.	St.dev.
Vt12	3.9.2013	5410	126_3034	5.3	4.2	3.2	0.32
Vt3	11.8.2013	5325	139_4266	5.5	3.9	2.9	0.34
			139_4286	5.2	1.6		

7.2.3 *Influence of calibration model form*

Due to the use of a single data point and the exponential mathematical form for the relationship between the air voids and dielectric constant, the implication is that the air voids variation is lost in the calibration process.

This is illustrated in Figure 62 below, where an average of all 27 cores (2.2 %) was matched to the stationary and continuous GPR measurements for Vt3. Similarly, at Vt12 the average air voids of all 10 cores (4.2 %) was matched to the stationary dielectric constant and average of continuous measurements. Factor $k = 1$ represents the original laboratory measurements using Percometer.

Figure 62 shows that the higher the value of ε_r' is, the lower the calibration factor k is. The low values of k will produce less variation for the air void content than the original equation because of the exponential form. This is particularly true for the low air void contents. This explains the nonrealistic low standard deviations obtained for the calibrated air void content values relative to the conventional water-air measurements, discussed in Section 3.4.2.

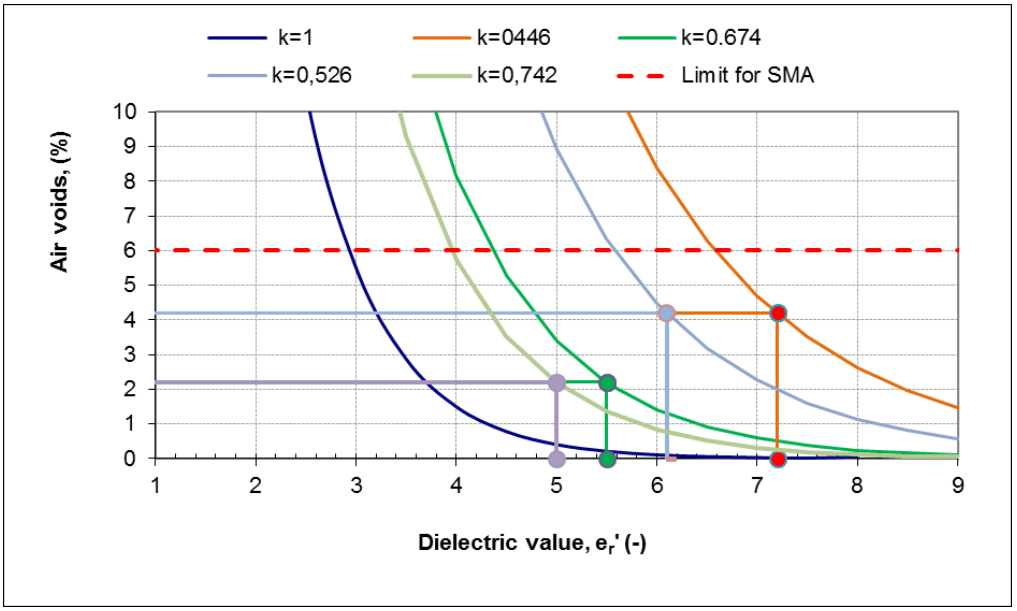

	Vt3 (20 h)		Vt12 (76 d)	
Cores	Stationary (both WPs)	Continuous (both WPs)	Stationary (RWP)	Continuous (both WPs)
Avg. (St.dev.) air voids (%)	2.2 (0,56)	2.2 (0.56)	4.2	4.2
Avg. (St.dev.) ε_r' (-)	5.5 (0,12)	5.0 (0.17)	7.2 (0,30)	6.1 (0.37)
Computed k value	0.674	0.742	0.446	0.526

Figure 62. *Effect of calibration factor k on standard deviation of air voids (precision).*

7.3 Variation in measurements

The variation (precision) of dielectric constant measurements was studied for the laboratory and GPR measurements. The following preliminary conclusions can be drawn:

- The standard deviation of the dielectric constant ε_r' was 0.04-0.06 units. This represents the testing variation of the electromagnetic method itself for the VNA transmission method, cavity resonator and circular waveguide cut-off methods.
- The standard deviation of rock aggregate ε_r' for testing a solid rock slab from various discrete points was 0.24. This represents combined material and testing variation. Material variation derived from varying mineralogy and was dependent on the rock type.
- The standard deviation of asphalt ε_r', for testing a thin slab with the VNA transmission method, was ca. 1.0. This represents the combined material and testing variation. For asphalt mixture with air-granule variation, the testing variation seems to be increased by the testing arrangement when 7 to 17 GHz frequency range was applied.
- The 7 to 17 GHz VNA point measurements of 150-mm pavement cores gave testing variation ranging from 0.04 to 0.96. It was obvious that the dimensions and homogeneity of the core affected results. Large aggregates seemed to dominate readings.
- Resolution to the GPR equipment is reported as being 0.1 units. The stationery measurements offered the ε_r' standard deviation of 0.04 to 0.06 for Vt3 and 0.12 to 0.16 for Vt12. These represent testing variation without the material variation and are comparable to the laboratory results for the attainable resolution of the electromagnetic measurement method.
- When the GPR is moving, it starts to pick up the material variation coming from the pavement layers and the geometry of the structure. Continuous measurements indicated that this variation ranged from 0.13 to 0.18 on Vt3 when measured after 20 h, 6 days and 40 days of construction.
- For Vt12, were measurements were taken 76 days after construction, variation ranged from 0.33 to 0.40. Permittivity values increased towards the end of the test section, and it is not known if this increase was due to moisture or some structural aspects of the pavement layers.
- Moisture in the pavement increased the measured ε_r' variation. For Vt3, the old pavement surface gave the standard deviation of 0.37 which was ca. double than for the dry pavement. The average SSD air void content at core location was 2.2 % of air.

8 CONCLUSION

The overall objective of this study is to investigate whether the existing GPR technique used in Finland is accurate enough to be used as a Quality Control (QC)/Quality Assurance (QA) tool in assessing the compaction of newly laid asphalt pavements. The work included field and laboratory experiments as well as a review of the existing PANK calibration method for the GPR measurements.

Field experiments were conducted in the autumn of 2013 in real conditions on highways Vt3 and Vt12 near the City of Tampere. The test road had two lanes for one direction and roads were paved with the Stone Mastic Asphalt mixture SMA16. Roads were paved with an approx. 40 mm thick new asphalt layer. A total of 36 cores and 2 slabs were obtained from the roads and tested in the laboratory for the air void contents. In addition, raw materials were collected from the quarry and the asphalt plant for further permittivity studies. Roads were measured with GPR several times during the fall of 2013.

This report gives the findings of Phase I of the study, including GPR measurement analysis and laboratory experiments and sampling on test roads. GPR antennas of 2.2 GHz were used in the road measurements.

The accuracy of the GPR method has been questioned for two reasons: the method of calibration may inadvertently reduce density variations and cause systematic bias, which makes pavements appear to be more homogenous and dense than they actually are; secondly, the frequency range used may not have adequate depth resolution for separating the thin asphalt surface layer from the rest of the pavement structure.

The major findings from this Phase I of the study are:

- The PANK calibration method distorts the air void content variation and roads appear to be more homogeneous than they actually are. The true values (bias) depend on how well calibration core(s) represents the average density of the measured pavement layer. Because the actual density variation (precision) is artificially reduced, the probability of having single air void content values exceeding the limits set for the conventional air-water core measurements is practically almost zero.
- Increasing the number of calibration cores is not going to remedy the problem related to the precision of the method. The culprit is the calibration equation, which is not physically based and, therefore, cannot predict the actual dielectric variation of asphalt. The calibration factor k distorts the calculations, as it shifts the air void readings towards the higher ε_r' values, which decrease measurement variation further.
- Increasing the number of calibration cores may help in reducing the measurement bias, as the calibration process is highly sensitive to magnitude and the method of obtaining the air void content. If the moving average of the dielectric constant varies a lot and there are clear clusters of data, more cores may be needed along the length of the road.
- The method of obtaining air void content for cores has the paramount influence of the calibration process. The electromagnetic method measured all pavement types in a similar manner and the density variation reflects the “true volumetric” method of obtaining the bulk volume of voids in the asphalt pavement. The consequence is that the air-water volume method may give a false indication of the actual porosity of the road and its capacity to hold water in the pores.
- The SSD method used for obtaining air void content for SMA mixtures may give a false indication of the “true” air content of the pavement and its ability to collect water. If samples

have cavities, which allow water flow through the sample, the SSD gives an artificially low air void content for the core.

- Moisture in the pavement increases GPR measured ε_r' values due to the high permittivity of water, and these high readings are providing unrealistically low air void values. The ε_r' of a pavement should not exceed ε_r' of aggregate and bitumen—the maximum density of the material. If it does, there is moisture in the pavement. Therefore, all measurements should be done preferably within a week of paving work, but before any rainwater infiltrates the pavement. However, measurements should not be carried out on the same day as the mixture was placed down, not until the moisture introduced during production has had time to evaporate from the mixture.

- A theoretical simulation of the GPR measurement arrangement with 2.2 GHz antennas suggests that there is a difference of 0.3 units in the measured ε_r' value, when a 40 mm thick surface layer with ε_r' of 5.0 is placed over an infinite thick asphalt base layer of ε_r' 4.0. The combined ε_r' was 4.7. Most likely, this difference contributes to both sources of testing variation, precision and a systematic bias.

The next step in the study is to propose a better calibration method based on further analysis of the GPR data and laboratory experiments. In addition, follow-up GPR measurements should be conducted in Vt 3 and Vt 12 to verify the evolution of permittivity and the thickness of pavement layers. For these measurements, new calibration cores should be extracted from the vicinity of the old cores.

REFERENCES

Al-Qadi. I., Lahouar. S., Loulizi, A. In situ measurements of hot-mix asphalt dielectric properties. NDTE & International. 2001, 34. pp 427-434.

Annan AP. Ground penetrating radar: Principles, procedures & applications. Mississauga: Sensors & Software Inc.; 2003.

American Association of State Highway and Transportation Officials (AASHTO), Standard Specification for Performance Graded Asphalt Binders M320, 2010.

Barton, D. Radar system analysis and modeling. Artech House, Norwood, 2005, pp. 198-201.

Currie, N. (ed). Techniques of radar reflectivity measurements, Artech House, Norwood. 1984, pp. 109-132.

Fauchard, C., Li, B., Laguerre, L., Héritier, B., Benjelloun, N., Kadi, M. Determination of the compaction of hot mix asphalt using high-frequency electromagnetic methods, NDT & E International, Vol 60, December 2013, pp. 40-51.

Finnish Asphalt Specifications 2000, Finnish Pavement Technology Advisory Council (PANK), Edita Ltd, Helsinki, 2000, ISBN 951-97197-6-8

Finnish Asphalt Specifications 2008. Finnish Pavement Technology Advisory Council, (PANK), Edita Ltd, Helsinki, 2007, ISBN 978-952-99985-0-0

Huuskonen-Snicker, E., Eskelinen, P., Pellinen, T., Olkkonen, M-K. A methodology of independent evaluation of magnetic and dielectric properties of rock specimens utilizing radio frequencies. 2015, *Submitted*, Hyyppä, H,J. Asfalttipäällysteiden koostumuksen tasalaatuisuus. Doctoral thesis. Helsinki University of Technology, Espoo, 2000.

Lahouar, S. Development of Data analysis algorithms for interpretation of ground penetrating radar Data. Thesis Blacksburg, Virginia, 2003.

Leng, Z. Prediction of in-situ asphalt mixture density using ground penetrating radar: theoretical development and field verification. Doctoral dissertation. University of Illinois at Urbana-Champaign, Illinois, 2011.

Leng. Z, Al-Qadi. I., Lahouar. S. Development and validation for in situ asphalt mixture density predictions models. NDT&E International 2011, 44. pp 369-375.

Loizos. A., and Plati. C. Assessment of HMA Air-Voids and Stiffness Based on Material Dielectric Values. Road Materials and Pavement Design, 2011, 12:1, 217-226.Narbro, A. et al. Mara Nord Project Final Report. Rovaniemi University of Applied Sciences, 2012. http://maranord.ramk.fi/static/content_files/Final_Report_Mara_Nord_Project_2012.pdf

Nelson SO. Density-permittivity relationships for powdered and granular materials. IEEE T Instrum Meas 2005;54:2033–2040.

Nevalainen, N. The use of thermal camera for quality assurance of asphalt pavement construction, Master's thesis, Aalto University, 2014. Olkkonen, M.-K., Eskelinen, P., Huuskonen-Snicker, E., Pellinen, T. Computerized microwave asphalt scanner. 2014. *Submitted.*

Olkkonen, M-K., Eskelinen, P., Huuskonen-Snicker, E., Pellinen, T. and Olmos Martinez, P. An Evaluation of the Permittivity of Two Different Rock Types Using Microwave Resonator and Waveguide Cutoff Principles. De Gruyter. Frequenz, 69, 1-2, 75–82, 2015.

Peisa, K. and Poikajärvi J. Mara Nord project WP 5 Final Report. Rovaniemi University of Applied Sciences, 2012. http://maranord.ramk.fi/static/content_files/WP5_Final_Report.pdf

Pellinen, T., Kutczek, T. Methodology of Assessing Testing Variability in Hot Mix Asphalt Production. ASTM Journal of Testing and Evaluation, Vol. 35, Issue 3, May 2007.

Pellinen, T. Asfalttimassan epähomogeenisuuden ja lajittumisen vaikutuksesta asfalttipäällysteeseen. Master's thesis, University of Oulu, Finland, 1985.Ramo, S. and Whinnery, J. Fields and Waves in modern radio. 2nd ed. John Whiley and Sons, NY 1960, pp. 288-311.

Roimela, P. Päällystetutkatutkimukset 1996-1997, Tiehallinno selvityksiä 4/1998. Rovaniemi, 1997.

Saarenketo, T. Electrical properties of road materials and subgrade soils and the use of Ground Penetrating Radar in traffic infrastructure surveys. Doctoral dissertation. University of Oulu, Finland, 2006.

Scheer, J. Radar reflectivity calibration procedures. In Techniques of radar reflectivity measurement, Nicholas Currie (ed.), Artech House, Norwood, 1983. pp. 109–132.

Stroup-Gardiner, M. and Brown, E. Segregation in Hot-Mix Asphalt Pavements. National Co-operative highway Research Program. Report No. 441. Auburn University, 2000.Terman, F. Electronic and Radio Frequencies. McGraw-Hill, NY, 1955. pp. 913-924-

Terman, F. Electronic and Radio Frequencies. McGraw-Hill, NY, 1955, pp. 913-924.

Appendix A: Vt3 pavement structure

V3 KEHÄ II - PÄÄLLYSRAKENTEEN PERIAATEKUVA
(ei mittakaavassa)

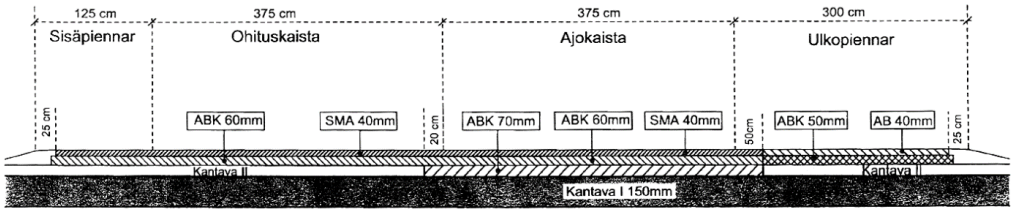

Louherakenne

Appendix B: Statistical definitions and resolution

The sources of variability in the realization of a test method according to the standard practice procedures of American Society of Testing and Materials (ASTM): ASTM E177 "Use of Terms Precision and Bias in ASTM Test Methods" are operator, apparatus, environment, sample (sampling), and time. The variability may include systematical as well as random components. The systematic components may be evaluated if an accepted reference value is available.

The following definitions for precision, bias, accuracy, repeatability and reproducibility have been reproduced from ASTM E456: "Standard Terminology for Relating to Quality and Statistics" and ASTM E177. The relationships among bias, precision, and accuracy are illustrated in Figure 1.

Precision (hajonta tai sisäinen tarkkuus)
The closeness of agreement between independent test results obtained under stipulated conditions.

Bias (harha tai poikkeama)
The difference between the expectation of the test results and an accepted reference value.

Accuracy (ulkoinen tarkkuus)
The closeness of agreement between a test result and an accepted reference value. The term accuracy, when applied to a set of test results, involves a combination of a random component and of a common systematic error or bias component.

Repeatability (toistettavuus)
Precision under repeatability conditions. Repeatability conditions: conditions where independent test results are obtained with the same method on identical test items in the same laboratory by the same operator using the same equipment within short intervals of time.

Reproducibility (uusittavuus)
Precision under reproducibility conditions. Reproducibility conditions: conditions where test results are obtained with the same method on identical test items in different laboratories with different operators using different equipment.

Resolution (resoluutio)
The smallest detectable increment that an instrument will measure/display to.

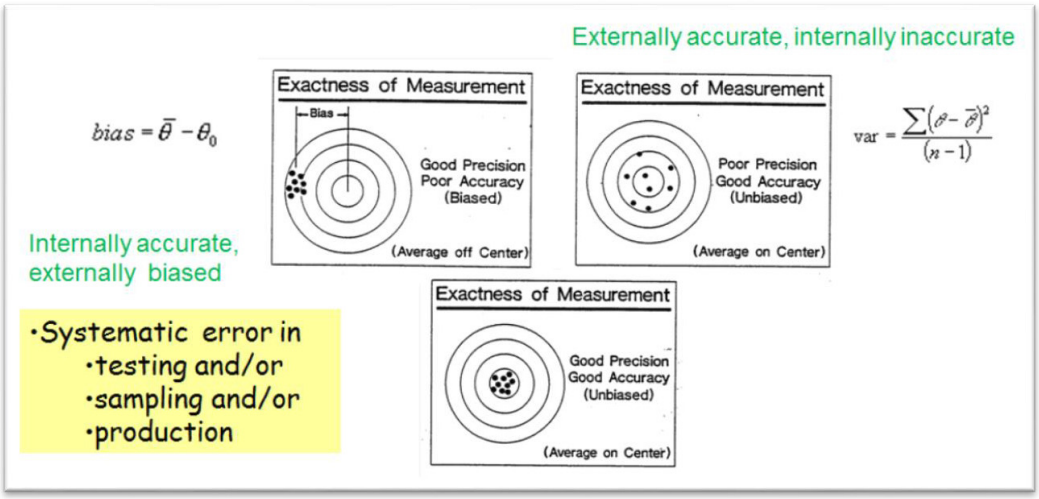

Figure 1. *Precision, bias and accuracy.*

This research has been conducted in collaboration with Liikennevirasto (Finnish Transport Agency).

Aalto-ST 9/2015

ISBN 978-952-60-6288-4 (pdf)
ISSN-L 1799-4896
ISSN 1799-4896 (printed)
ISSN 1799-490X (pdf)

Aalto University
School of Engineering
Department of Civil and Environmental Engineering
www.aalto.fi

BUSINESS + ECONOMY

ART + DESIGN + ARCHITECTURE

SCIENCE + TECHNOLOGY

CROSSOVER

DOCTORAL DISSERTATIONS